**Supporting Information**

# Catalytic Carbodiimide Guanylation by a Nucleophilic, High Spin Iron(II) Imido Complex

Yafei Gao, Veronica Carta, Maren Pink, and Jeremy M. Smith*

Department of Chemistry, Indiana University, 800 East Kirkwood Avenue, Bloomington, Indiana 47405, United States

## Contents

## Experimental

**General Considerations.** All manipulations were performed under a nitrogen atmosphere by standard Schlenk techniques or in an MBraun glove box. Glassware was dried at 130 °C overnight before cooling under a dynamic vacuum in an antechamber. Diethyl ether ($Et_2O$), tetrahydrofuran (THF), toluene, and pentane were purified by a PPT solvent purification system. Celite was dried overnight at 130 °C under vacuum. Potassium graphite ($KC_8$)[1], [$Ph_2B(^tBuIm)_2Fe(\eta^6$-toluene)][2], [$Ph_2B(^tBuIm)_2FeCl(THF)$][2], 2,6-diisopropylphenyl azide ($DippN_3$)[3] and 2,6-diisopropylphenylamide potassium (DippNHK)[4] were synthesized according to literature procedures. All other chemicals were purchased and used as received. $^1$H NMR spectroscopic data were recorded on Varian spectrometers. Solution magnetic susceptibilities were determined by Evans' method.[5] UV-Vis spectroscopic data were collected on an Agilent Technologies Cary 60 UV-Vis instrument.

$^{57}$Fe Mössbauer spectra were recorded on a SEE Co spectrometer. The sample temperature was controlled using a SVT-400 Dewar from Janis equipped with a Lake Shore 255 Temperature Controller. The isomer shifts are reported relative to the centroid of the spectrum of α-Fe at 298 K. Samples were prepared by grinding crystallized material into a fine powder and then mounting in a cup, plugged with a fitted O-ring sealed cap. Data analysis was performed using the program WMOSS[6] and quadrupole doublets were fitted to Lorentzian lineshapes. Elemental analysis was conducted by Midwest Microlab, LLC (Indianapolis, IN). GC/MS analysis was performed using an Agilent 6890N gas chromatograph and 5973 inert mass-selective detector equipped with a DB-5MS (Agilent) column (30 m × 0.25 mm). Mass spectra were recorded using negative/positive electrospray ionization on a Thermo Electron Corp MAT-95XP spectrometer.

**$Ph_2B(^tBuIm)_2FeNDipp$ (1).** A vial was charged with [$Ph_2B(^tBuIm)_2Fe(\eta^6$-toluene)] (388 mg, 0.69 mmol) and THF (5 mL). The solution was cooled to -35 °C. Liquid 2,6-Diisopropylphenyl azide ($DippN_3$) (141 mg, 0.69 mmol) was added and the mixture allowed to warm to room temperature. The solution became dark green over the course of 4 h stirring. The THF was removed under vacuum, affording a dark green residue that was washed with pentane (3 × 5 mL) to give [$Ph_2B(^tBuIm)_2FeNDipp$] (**1**) as a dark green powder (297 mg, 66% yield). Crystals suitable for X-ray diffraction were grown by diffusing pentane into a toluene solution of **1** at room temperature. $^1$H NMR (400 MHz, THF-$d_8$, 25 °C): $\delta$ (ppm) 94.5 ($\nu_{1/2}$ = 172 Hz), 82.2 ($\nu_{1/2}$ = 194), 16.2 ($\nu_{1/2}$ = 201 Hz), 9.9 ($\nu_{1/2}$ = 402 Hz), 3.2 ($\nu_{1/2}$ = 96 Hz), 0.3 ($\nu_{1/2}$ = 76 Hz), -21.9 ($\nu_{1/2}$ = 124 Hz), -67.3 ($\nu_{1/2}$ = 565 Hz). $\mu_{eff}$ (Evans', THF-$d_8$, 25 ˚C): 4.2(2) $\mu_B$. UV-vis (THF, 25 ˚C): $\lambda_{max}$, nm ($\varepsilon$, $M^{-1}cm^{-1}$) = 447 (3092), 620 (2042). Anal. Calcd. for $C_{38}H_{49}BFeN_5$: C 71.04, H 7.69, N 10.90. Found C 70.93, H 7.67, N 10.79.

**$[Ph_2B(^tBuIm)_2FeNDipp][K(18\text{-}C\text{-}6)THF_2]$ (2).** A vial was charged with $Ph_2B(^tBuIm)_2FeNDipp$ (**1**) (580 mg, 0.90 mmol) and THF (5 mL). The solution was cooled to -78 °C. Solid $KC_8$ (146 mg, 1.08 mmol) and 18-crown-6 (238 mg, 0.90 mmol) were sequentially added and the mixture was allowed to warm to room temperature. The solution turned red over the course 4 h stirring. The solution was filtered through Celite and concentrated under vacuum to afford a red residue that was washed with pentane (3 × 5 mL) to give [$Ph_2B(^tBuIm)_2FeNDipp$][K(18-C-6)$THF_2$] (**2**) as a red powder (785 mg, 80% yield). Crystals suitable for X-ray diffraction were grown at -35 ˚C from a concentrated THF solution that was layered with pentane. $^1$H NMR (400 MHz, THF-$d_8$, 25 °C): $\delta$ (ppm) 123.9 ($\nu_{1/2}$ = 268 Hz), 96.9 (very broad), 32.6 ($\nu_{1/2}$ = 374 Hz), 29.9 ($\nu_{1/2}$ = 94 Hz), 17.6 ($\nu_{1/2}$ = 229 Hz), 5.8 ($\nu_{1/2}$ = 37 Hz), 2.9 ($\nu_{1/2}$ = 44 Hz), -99.5 ($\nu_{1/2}$ = 581 Hz). $\mu_{eff}$ (Evans', THF-$d_8$, 25 ˚C): 5.0(1) $\mu_B$. UV-vis (THF, 25 ˚C): $\lambda_{max}$, nm ($\varepsilon$, $M^{-1}cm^{-1}$) = 290 (10375), 331 (8040), 426 (2223).

Despite several attempts, we have been unable to obtain satisfactory elemental analysis for this complex, likely due to its thermal instability. For example, the complex decomposes upon standing in room temperature solution, as indicated by a change in color from red to brownish yellow overnight. The resulting $^1$H NMR spectrum reveals a plethora of unknown compounds, although $DippNH_2$ can be observed by GC-MS.

**$[Ph_2B(^tBuIm)_2Fe(NHDipp)_2][K(18\text{-}C\text{-}6)THF_2]$ (3).** Method A. A vial was charged with $[Ph_2B(^tBuIm)_2FeNDipp][K(18\text{-}C\text{-}6)THF_2]$ (**2**) (205 mg, 0.19 mmol) and THF (5 mL). Liquid 2,6-Diisopropylaniline ($DippNH_2$) (33 mg, 0.19 mmol) was added and the mixture stirred at room temperature overnight. The solution became brownish yellow over the course of the reaction. The THF was removed under vacuum, affording a brownish yellow residue that was washed with pentane (3 × 5 mL) to give $[Ph_2B(^tBuIm)_2Fe(NHDipp)_2][K(18\text{-}C\text{-}6)THF_2]$ (**3**) as a yellow powder (210 mg, 88% yield). Crystals suitable for X-ray diffraction were grown at -35 ˚C from a concentrated THF solution that was layered with pentane. $^1$H NMR (400 MHz, THF-$d_8$, 25 °C): $\delta$ (ppm) 34.3 ($\nu_{1/2}$ = 244 Hz), 26.5 ($\nu_{1/2}$ = 122), 16.5 ($\nu_{1/2}$ = 151 Hz), 14.0 ($\nu_{1/2}$ = 694 Hz), 8.1 (broad), 7.50 (broad), 7.26 (broad), 3.7 ($\nu_{1/2}$ = 17), -0.9 ($\nu_{1/2}$ = 54), -53.9 ($\nu_{1/2}$ = 53 Hz). $\mu_{eff}$ (Evans', THF-$d_8$, 25 ˚C): 5.4(2) $\mu_B$. UV-vis (THF, 25 ˚C): $\lambda_{max}$, nm ($\varepsilon$, $M^{-1}cm^{-1}$) = 290 (21843), 327 (19636), 427 (3816). Anal. Calcd. for $C_{70}H_{108}BFeKN_6O_8$: C 66.34, H 8.59, N 6.63. Found C 66.76, H 8.93, N 7.16. Method B. A vial was charged with $Ph_2B(^tBuIm)_2FeCl(THF)$ (370 mg, 0.64 mmol) and THF (5 mL). Solid DippNHK (276 mg, 1.28 mmol) and 18-crown-6 (337 mg, 1.28 mmol) were sequentially added. The solution turned brownish yellow over the course 2 h stirring. The solution was filtered through Celite and concentrated under vacuum to afford a yellow residue that was washed with pentane (3 ×5 mL) to give $[Ph_2B(^tBuIm)_2Fe(NHDipp)_2][K(18\text{-}C\text{-}6)THF_2]$ (3) as a

yellow powder (689 mg, 85% yield). The $^1$H NMR of the sample prepared in this way is identical to that prepared via method A.

**[Ph$_2$B($^t$BuIm)$_2$Fe($^i$PrN)$_2$CNDipp][K(18-C-6)THF$_2$] (4).** A vial was charged with [Ph$_2$B($^t$BuIm)$_2$FeNDipp][K(18-C-6)THF$_2$] (**2**) (342 mg, 0.31 mmol) and THF (5 mL). Liquid *N, N′*-Diisopropylcarbodiimide ($^i$PrNCN$^i$Pr) (40 mg, 0.31 mmol) was added and the mixture stirred at room temperature overnight. The solution became brownish yellow over the course of the reaction. The THF was removed under vacuum, affording a brownish yellow residue that was washed with pentane (3 × 5 mL) to give [Ph$_2$B($^t$BuIm)$_2$Fe($^i$PrN)$_2$CNDipp][K(18-C-6)THF$_2$] (**4**) as a yellow powder (352 mg, 92% yield). Crystals suitable for X-ray diffraction were grown at -35 °C from a concentrated THF solution that was layered with pentane. $^1$H NMR (400 MHz, THF-$d_8$, 25 °C): $\delta$ (ppm) 26.4 ($\nu_{1/2}$ = 159 Hz), 19.2 ($\nu_{1/2}$ = 453), 12.1 ($\nu_{1/2}$ = 70 Hz), 6.5 ($\nu_{1/2}$ = 86 Hz), 4.9 (broad), 4.6 (very broad), 3.3 (broad), 1.3 (broad), 1.1 (broad), 0.9 ($\nu_{1/2}$ = 38 Hz), -7.8 ($\nu_{1/2}$ = 387 Hz). $\mu_{eff}$ (Evans', THF-$d_8$, 25 °C): 5.0(1) $\mu_B$. UV-vis (THF, 25 °C): $\lambda_{max}$, nm ($\varepsilon$, $M^{-1}cm^{-1}$) = 267 (19477), 284 (16559), 432 (2175). Anal. Calcd. for $C_{69}H_{111}BFeKN_7O_9$: C 64.32, H 8.68, N 7.61. Found C 63.03, H 8.42, N 7.15.

**Equilibrium constant determination**

A J-Young tube was charged with [Ph$_2$B($^t$BuIm)$_2$Fe(NHDipp)$_2$][K(18-C-6)THF$_2$] (**3**) (22 mg, 0.017 mmol) and THF-$d_8$ (0.5 mL),Mesitylene (6 mg, 0.05 mmol) was added as an internal standard. Equilibration was monitored by $^1$H NMR (at 25 °C), providing equilibrium concentrations of [[Ph$_2$B($^t$BuIm)$_2$Fe(NHDipp)$_2$][K(18-C-6)THF$_2$]] = 0.021 mol/L, [[Ph$_2$B($^t$BuIm)$_2$FeNDipp][K(18-C-6)THF$_2$]] = 0.013 mol/L and [DippNH$_2$] = 0.013 mol/L. (see Figure S17).

These data provide an equilibrium constant for the reaction: .

$[Ph_2B(^tBuIm)_2Fe(NHDipp)_2]^- \leftrightarrows [Ph_2B(^tBuIm)_2Fe(NDipp)]^- + H_2NDipp \quad K_{eq} \approx 8 \times 10^{-3}$ mol/L

**Reaction of $[Ph_2B(^tBuIm)_2Fe(^iPrN)_2CNDipp][K(18\text{-}C\text{-}6)THF_2]$ (4) with $DippNH_2$.** A J-Young tube was charged with $[Ph_2B(^tBuIm)_2Fe(^iPrN)_2CNDipp][K(18\text{-}C\text{-}6)THF_2]$ (**4**) (40 mg, 0.033 mmol), $DippNH_2$ (23 mg, 0.13 mmol) and THF-$d_8$ (0.5 mL). The reaction was monitored by $^1H$ NMR. Complete consumption of $[Ph_2B(^tBuIm)_2Fe(^iPrN)_2CNDipp][K(18\text{-}C\text{-}6)THF_2]$ (**4**) with concomitant formation of $[Ph_2B(tBuIm)_2Fe(NHDipp)_2][K(18\text{-}C\text{-}6)THF_2]$ (**3**) occurred over 72 h at room temperature, as determined by $^1H$ NMR spectroscopy (see Figure S18). The organic product *N*-2,6-diisopropylphenyl-*N′*, *N″*-diisopropylguanidine was characterized by $^1H$ NMR spectroscopy and further confirmed by GC-MS.

**Reaction of $[Ph_2B(^tBuIm)_2Fe(NHDipp)_2][K(18\text{-}C\text{-}6)THF_2]$ (3) with *N, N′*-diisopropylcarbodiimide.** A J-Young tube was charged with $[Ph_2B(tBuIm)_2Fe(NHDipp)_2][K(18\text{-}C\text{-}6)THF_2]$ (**3**) (35 mg, 0.027 mmol), *N,N′*-Diisopropylcarbodiimide (14 mg, 0.11 mmol) and THF-$d_8$ (0.5 mL). Complete consumption of $[Ph_2B(^tBuIm)_2Fe(NHDipp)_2][K(18\text{-}C\text{-}6)THF_2]$ (**3**) with concomitant formation of $[Ph_2B(^tBuIm)_2Fe(^iPrN)_2CNDipp][K(18\text{-}C\text{-}6)THF_2]$ (**4**) occurred over 30 h, as determined by $^1H$ NMR spectroscopy (see Figure S19).

**General procedure for the catalytic guanylation of carbodiimides.** A vial was charged with complexes **2**, **3** or **4** (5 mol%, 0.05 mmol), carbodiimide (1.1 mmol), aniline (1.0 mmol) and THF (2.0 mL). The solution was stirred at room temperature and the reaction monitored by GC-MS. Upon completion, the volatiles were removed *in vacuo*, the residue extracted with ether and filtered through Celite to give a clear solution. After removal of the solvent under vacuum, the guanidine products were further purified by washing with cold pentane.

For substrates 4-aminobenzonitrile and methyl 4-aminobenzoate: A J-Young tube was charged with complex **2** (5 mol%), carbodiimide (0.15 mmol), aniline (0.1 mmol) and THF-$d_8$ (0.5 mL). The mixture was monitored by $^1$H NMR spectroscopy at room temperature. After complete consumption of aniline, mesitylene (0.1 mmol) was added as the internal standard to quantify the guanidine products. The products were further confirmed by GC-MS.

**Characterization data for guanidine product:**

***N*-2,6-diisopropylphenyl-*N′*, *N″*-diisopropylguanidine**

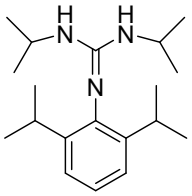

White solid (243 mg, 80% yield).

$^1$H NMR (400 MHz, $CDCl_3$, 25 $^o$C): $\delta$ (ppm) 7.07 (d, $J$ = 8.0 Hz, 2H), 6.97 (t, $J$ = 8.0 Hz, 1H), 4.20 (bs, 1H), 3.41-3.22 (b, 3H), 3.09 (m, 2H), 1.16 (m, 24H). $^{13}$C NMR (101 MHz, $CDCl_3$, 25 $^o$C): $\delta$ (ppm) 147.47, 144.12, 141.33, 122.93, 122.00, 43.17, 42.46, 27.80, 23.66. These data are in accordance with the literature.[7]

***N*-2,6-diisopropylphenyl-*N′*, *N″*-dicyclohexylguanidine**

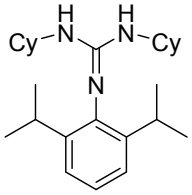

White solid (318 mg, 83% yield).

$^{1}$H NMR (400 MHz, $CDCl_3$, 25 $^{o}$C): $\delta$ (ppm) 7.06 (d, $J$ = 8.0 Hz, 2H), 6.95 (t, $J$ = 8.0 Hz, 1H), 3.90 (bs, 1H), 3.45-3.30 (b, 2H), 3.09 (m, 2H), 2.97 (b, 1H), 2.12-1.86 (b, 4H), 1.61-1.68 (b, 6H), 1.34 (b, 4H), 1.16-1.14 (m, 18H). $^{13}$C NMR (101 MHz, $CDCl_3$, 25 $^{o}$C): $\delta$ (ppm) 147.21, 144.22, 141.35, 122.90, 121.93, 50.61, 49.05, 34.24, 27.79, 25.75, 25.03, 23.65. These data are in accordance with the literature.[8]

***N*-2,4,6-trimethylphenyl-*N′*, *N″*-diisopropylguanidine**

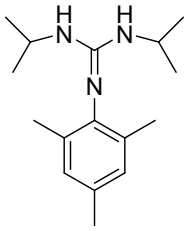

White solid (227 mg, 87% yield).

$^{1}$H NMR (400 MHz, $CDCl_3$, 25 $^{o}$C): $\delta$ (ppm) 6.80 (s, 2H), 4.15 (bs, 2H), 3.37 (bs, 2H), 2.22 (s, 3H), 2.06 (s, 6H), 1.15 (b, 12H). $^{13}$C NMR (101 MHz, $CDCl_3$, 25 $^{o}$C): $\delta$ (ppm) 147.84, 143.61, 130.53, 130.40, 128.50, 43.09, 23.58, 20.71, 18.10. These data are in accordance with the literature.[9]

***N*-2,4,6-trimethylphenyl-*N′*, *N″*-dicyclohexylguanidine**

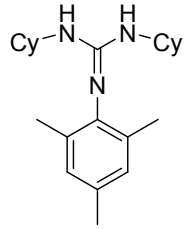

White solid (279 mg, 82% yield).

$^{1}$H NMR (400 MHz, $CDCl_3$, 25 $^{o}$C): $\delta$ (ppm) 6.78 (s, 2H), 3.87 (bs, 1H), 3.35 (b, 2H), 2.97 (bs, 1H), 2.21 (s, 3H), 2.06 (s, 6H), 1.86 (b, 2H), 1.67-1.58 (m, 6H), 1.34-0.95 (m, 12H). $^{13}$C NMR (101 MHz, $CDCl_3$, 25 $^{o}$C): $\delta$ (ppm) 147.65, 143.73, 130.60, 130.35, 128.49, 50.93, 49.20, 34.16, 25.74, 25.00, 20.72, 18.12. These data are in accordance with the literature.[10]

***N*-*o*-methoxyphenyl-*N′*, *N″*-diisopropylguanidine**

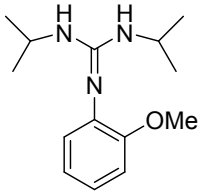

White solid (199 mg, 80% yield).

$^{1}$H NMR (400 MHz, $CDCl_3$, 25 $^{o}$C): $\delta$ (ppm) 6.92-6.84 (m, 4H), 3.77 (m, 5H), 3.50 (bs, 2H), 1.16 (d, $J$ = 4.0 Hz, 12H). $^{13}$C NMR (101 MHz, $CDCl_3$, 25 $^{o}$C): $\delta$ (ppm) 152.40, 150.36, 139.08, 124.72, 122.14, 121.29, 111.90, 55.60, 43.34, 23.37. These data are in accordance with the literature.[7]

***N*-*o*-methoxyphenyl-*N′*, *N″*-dicyclohexylguanidine**

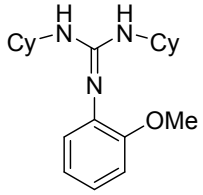

White solid (280 mg, 85% yield).

$^{1}$H NMR (400 MHz, $CDCl_3$, 25 $^{o}$C): $\delta$ (ppm) 6.93-6.83 (m, 4H), 3.76 (s, 3H), 3.56 (b, 2H), 3.44 (bs, 2H), 2.02-2.00 (m, 4H), 1.69-1.65 (m, 4H), 1.59-1.56 (m, 2H), 1.38-1.32 (m, 4H), 1.22-1.02 (m, 6H). $^{13}$C NMR (101 MHz, $CDCl_3$, 25 $^{o}$C): $\delta$ (ppm) 152.47, 150.16, 139.25, 124.57, 122.11, 121.30, 111.98, 55.65, 50.25, 33.83, 25.71, 24.89. These data are in accordance with the literature.[7]

***N*-*p*-methylphenyl-*N′*, *N″*-diisopropylguanidine**

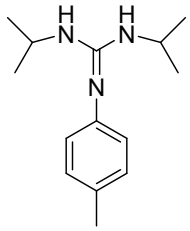

White solid (197 mg, 85% yield).

$^{1}$H NMR (400 MHz, $CDCl_3$, 25 $^{o}$C): $\delta$ (ppm) 7.04 (d, $J$ = 8.0 Hz, 2H), 6.75 (d, $J$ = 8.0 Hz, 2H), 3.91-3.74 (m, 4H), 2.28 (s, 3H), 1.15 (d, $J$ = 8.0 Hz, 12H). $^{13}$C NMR (101 MHz, $CDCl_3$, 25 $^{o}$C): $\delta$ (ppm) 150.59, 146.52, 130.79, 129.82, 123.21, 43.39, 23.29, 20.74. These data are in accordance with the literature.[8]

***N*-*p*-methylphenyl-*N′*, *N″*-dicyclohexylguanidine**

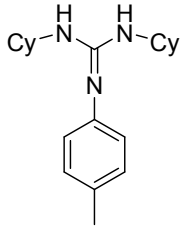

White solid (272 mg, 87% yield).

$^{1}$H NMR (400 MHz, $CDCl_3$, 25 $^{o}$C): $\delta$ (ppm) 7.03 (d, $J$ = 8.0 Hz, 2H), 6.73 (d, $J$ = 8.0 Hz, 2H), 3.61 (bs, 2H), 3.41 (bs, 2H), 2.27 (s, 3H), 2.01-1.98 (m, 4H), 1.70-1.66 (m, 4H), 1.60-1.57 (m, 2H), 1.39-1.30 (m, 4H), 1.22-1.04 (m, 6H). $^{13}$C NMR (101 MHz, $CDCl_3$, 25 $^{o}$C): $\delta$ (ppm) 150.08, 147.60, 130.32, 129.76, 123.31, 50.16, 33.83, 25.68, 24.90, 20.73. These data are in accordance with the literature.[8]

***N*-*p*-fluorophenyl-*N′*, *N″*-diisopropylguanidine**

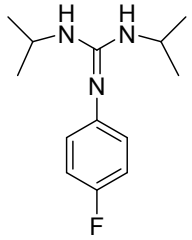

White solid (196 mg, 83% yield).

$^{1}$H NMR (400 MHz, $CDCl_3$, 25 $^{o}$C): $\delta$ (ppm) 6.95-6.90 (m, 2H), 6.78-6.75 (m, 2H), 3.75 (bs, 2H), 3.51 (bs, 2H), 1.15 (d, $J$ = 4.0 Hz, 12H). $^{13}$C NMR (101 MHz, $CDCl_3$, 25 $^{o}$C): $\delta$ (ppm) 158.19 (d, $J_{C\text{-}F}$ = 239.4 Hz), 150.41, 146.25 (d, $J_{C\text{-}F}$ = 2.0 Hz), 124.40 (d, $J_{C\text{-}F}$ = 7.1 Hz), 115.69 (d, $J_{C\text{-}F}$ = 22.2 Hz), 43.19, 23.32. These data are in accordance with the literature.[7]

***N*-*p*-fluorophenyl-*N′*, *N″*-dicyclohexylguanidine**

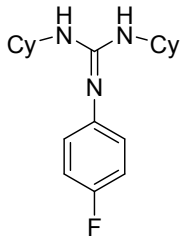

White solid (278 mg, 88% yield).

$^{1}$H NMR (400 MHz, $CDCl_3$, 25 $^{o}$C): $\delta$ (ppm) 6.94-6.90 (m, 2H), 6.79-6.75 (m, 2H), 3.58-3.56 (b, 2H), 3.40 (bs, 2H), 2.00-1.97 (m, 4H), 1.70-1.65 (m, 4H), 1.61-1.56 (m, 2H), 1.40-1.29 (m, 4H), 1.20-1.03 (m, 6H). $^{13}$C NMR (101 MHz, $CDCl_3$, 25 $^{o}$C): $\delta$ (ppm) 158.18 (d, $J_{C\text{-}F}$ = 239.4 Hz), 150.27, 146.39 (d, $J_{C\text{-}F}$ = 3.0 Hz), 124.48 (d, $J_{C\text{-}F}$ = 8.1 Hz), 115.67 (d, $J_{C\text{-}F}$ = 21.2 Hz), 50.11, 33.79, 25.63, 24.84. These data are in accordance with the literature.[7]

***N*-*p*-methoxyphenyl-*N′*, *N″*-diisopropylguanidine**

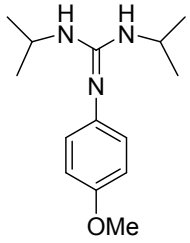

White solid (224 mg, 90% yield).

$^{1}$H NMR (400 MHz, $CDCl_3$, 25 $^{o}$C): $\delta$ (ppm) 6.82-6.75 (m, 4H), 3.77 (m, 5H, OC$\underline{H}_3$, C$\underline{H}$($CH_3$)$_2$), 3.51 (bs, 2H), 1.15 (d, $J$ = 8.0 Hz, 12H). $^{13}$C NMR (101 MHz, $CDCl_3$, 25 $^{o}$C): $\delta$ (ppm) 154.47, 150.57, 143.32, 124.17, 114.57, 55.40, 43.21, 23.37. These data are in accordance with the literature.[11]

***N*-*p*-trifluoromethylphenyl-*N′*, *N″*-dicyclohexylguanidine**

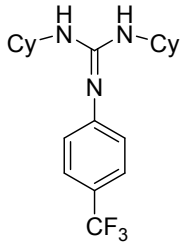

Pale yellow solid (300 mg, 82% yield).

$^{1}$H NMR (400 MHz, $CDCl_3$, 25 $^{o}$C): $\delta$ (ppm) 7.47 (d, $J$ = 8.0 Hz, 2H), 6.91 (d, $J$ = 8.0 Hz, 2H), 3.41 (m, 2H), 2.01-1.98 (m, 4H), 1.71-1.68 (m, 4H), 1.62-1.59 (m, 2H), 1.39-1.30 (m, 4H), 1.20-1.07 (m, 6H). $^{13}$C NMR (101 MHz, $CDCl_3$, 25 $^{o}$C): $\delta$ (ppm) 154.19, 149.82, 126.37, 123.38, 50.13, 33.71, 25.58, 24.85. $^{19}$F NMR (376 MHz, $CDCl_3$, 25 $^{o}$C): $\delta$ (ppm) -61.46. ESI-MS: m/z $[M-H]^-$ Calcd for $C_{20}H_{27}N_3F_3$ 366.2163; Found 366.2155.

***N*-*p*-methylsulfonylphenyl-*N′*, *N″*-diisopropylguanidine**

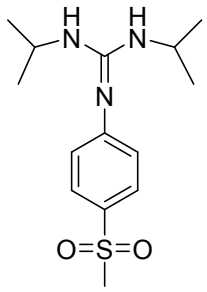

Yellow solid (206 mg, 70% yield).

$^{1}$H NMR (400 MHz, $CD_2Cl_2$, 25 $^{o}$C): $\delta$ (ppm) 7.72 (d, $J$ = 8.0 Hz, 2H), 6.94 (d, $J$ = 8.0 Hz, 2H), 3.90 (bs, 2H), 3.76 (bs, 2H), 3.00 (s, 3H), 1.15 (d, $J$ = 4.0 Hz, 12H). $^{13}$C NMR (101 MHz, $CD_2Cl_2$, 25 $^{o}$C): $\delta$ (ppm) 156.98, 150.55, 130.86, 128.74, 123.02, 44.78, 43.25, 22.91. ESI-MS: m/z $[M+H]^+$ Calcd for $C_{14}H_{24}N_3O_2S$ 298.1584; Found 298.1586.

**Supplementary Figures**

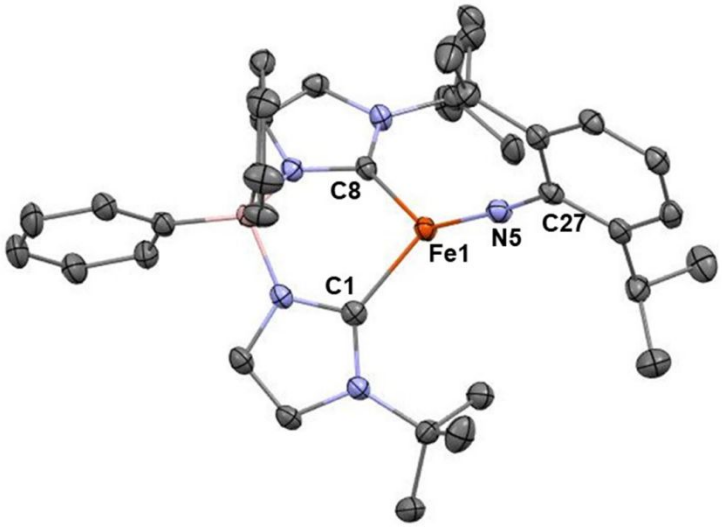


**Figure S1.** Molecular structure of [$Ph_2B(^tBuIm)_2FeNDipp$] (**1**), as determined by single crystal X-ray diffraction. Ellipsoids are shown at 50% probability level. Hydrogen atoms are omitted for clarity. Color scheme: C, dark gray; N, blue; B, pink; Fe, orange. Selected bond distances (Å) and angles (deg): Fe1-N5 1.708(2), Fe1-C1 2.013(2), Fe-C8 2.024(2); C1-Fe-C8 92.81(9), Fe1-N5-C27 172.3(2), C1-Fe1-N5 132.21(10), C8-F1e-N5 134.21(10).

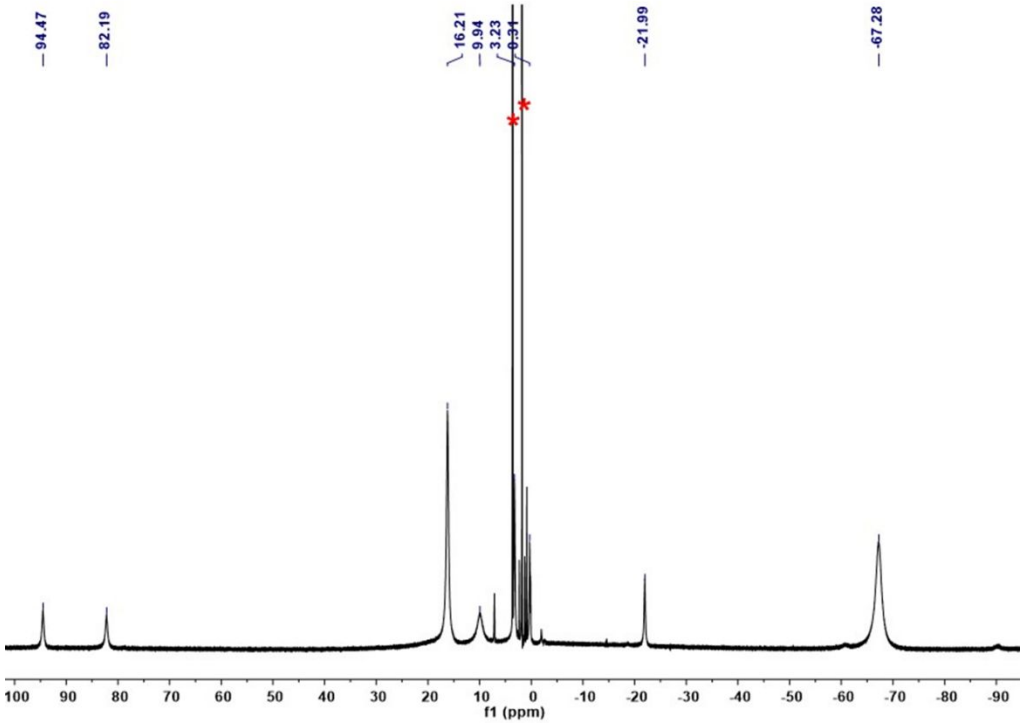


**Figure S2.** $^1H$ NMR spectrum (400 MHz, 25 °C, $d_8$-THF (*)) of [$Ph_2B(^tBuIm)_2FeNDipp$] (**1**).

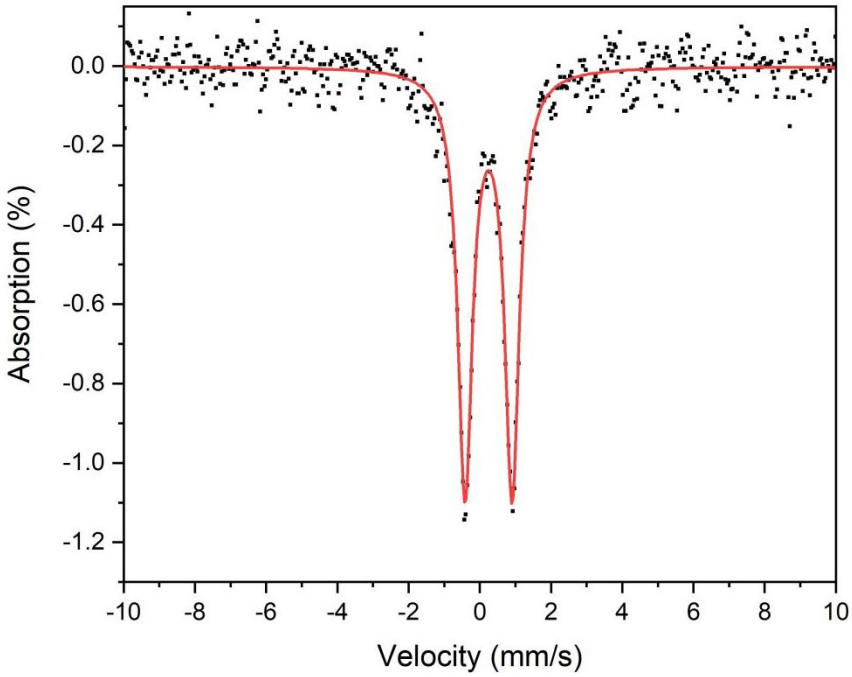


**Figure S3.** Zero-field $^{57}$Fe Mössbauer spectrum of [$Ph_2B(^tBuIm)_2FeNDipp$] (**1**) measured at 200 K. Parameters: $\delta$ = 0.25 mm/s, $\Delta E_Q$ = 1.32 mm/s.

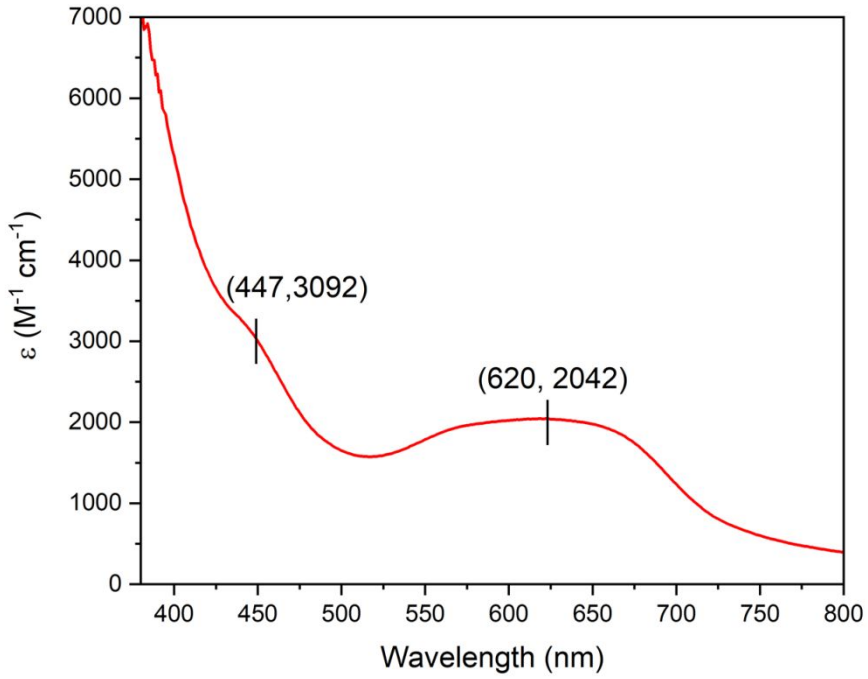


**Figure S4.** UV-vis spectrum of [$Ph_2B(^tBuIm)_2FeNDipp$] (**1**) measured at 25 °C in THF.

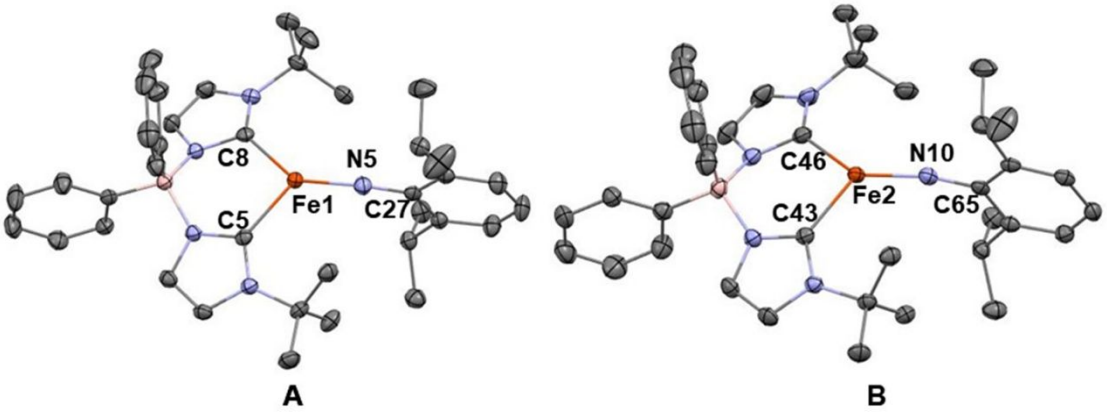


**Figure S5.** Molecular structure of $[Ph_2B(^tBuIm)_2FeNDipp][K(18\text{-}C\text{-}6)THF_2]$ (**2**), as determined by single crystal X-ray diffraction. Ellipsoids are shown at 50% probability level. Hydrogen atoms, counterions and solvent molecules are omitted for clarity. The compound crystalizes with two sets of molecules (Fe complex, counterion, and THF) in the asymmetric unit (Z'=2). Color scheme: C, dark gray; N, blue; B, pink; Fe, orange. Selected bond distances (Å) and angles (deg): Fe1-N5 1.777(2), Fe1-C5 2.087(2), Fe1-C8 2.081(2); C5-Fe1-C8 99.12(9), Fe1-N5-C27 172.64(19), C5-Fe1-N5 127.32(9), C8-Fe1-N5 128.00(10) in **A.** Fe2-N10 1.779(2), Fe2-C43 2.077(3), Fe2-C46 2.084(2); C43-Fe2-C46 98.15(9), Fe2-N10-C65 165.11(7), C43-Fe2-N10 129.77(9), C46-Fe2-N10 127.09(9) in **B**.

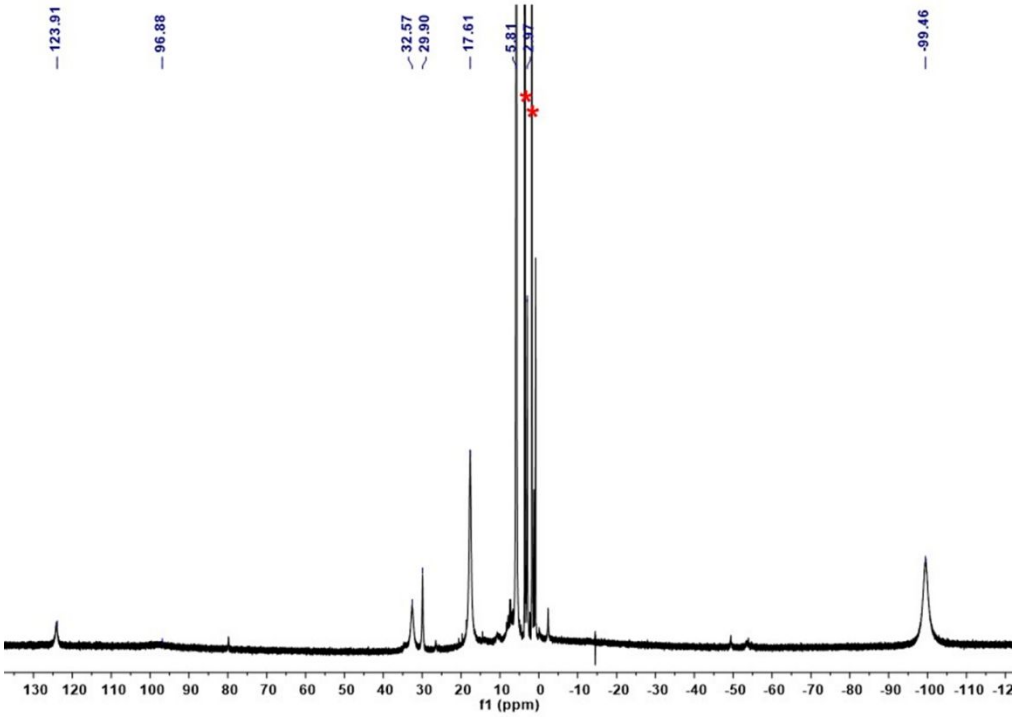


**Figure S6.** $^1H$ NMR spectrum (400 MHz, 25 °C, $d_8$-THF (*)) of $[Ph_2B(^tBuIm)_2FeNDipp][K(18\text{-}C\text{-}6)THF_2]$ (**2**).

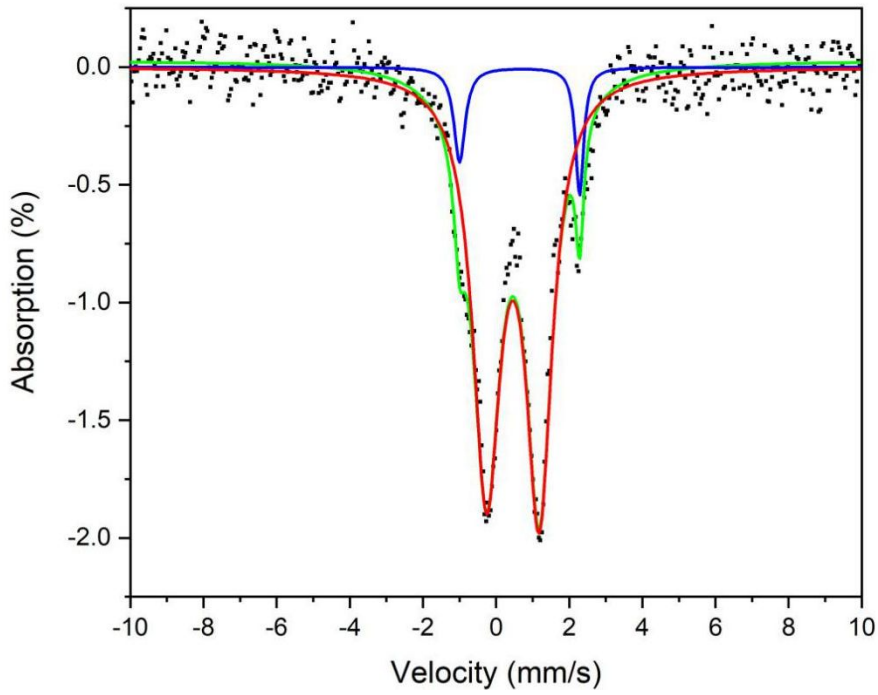


**Figure S7.** Zero-field $^{57}$Fe Mössbauer spectrum of [$Ph_2B(^tBuIm)_2FeNDipp$][K(18-C-6)$THF_2$] (**2**) measured at 80 K. Parameters: $\delta$ = 0.46 mm/s, $\Delta E_Q$ = 1.45 mm/s (major component, red line); $\delta$ = 0.64 mm/s, $\Delta E_Q$ = 3.28 mm/s (minor component, blue line, product resulting from the decomposition of **2** ).

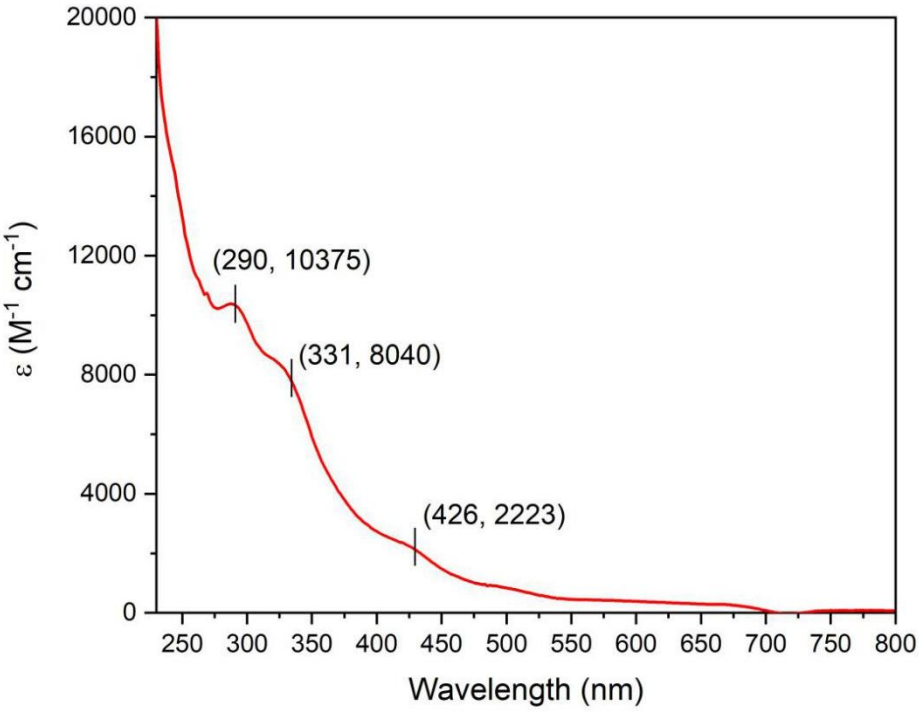


**Figure S8.** UV-vis spectrum of [$Ph_2B(^tBuIm)_2FeNDipp$][K(18-C-6)$THF_2$] (**2**) measured at 25 °C in THF.

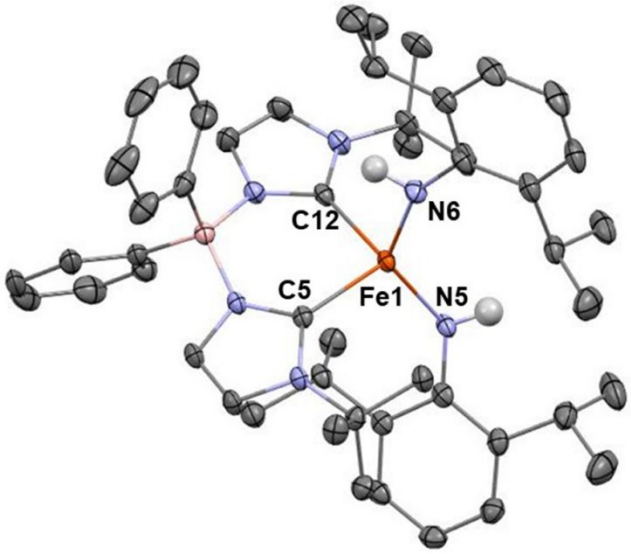


**Figure S9.** Molecular structure of $[Ph_2B(^tBuIm)_2Fe(NHDipp)_2][K(18\text{-}C\text{-}6)THF_2]$ (**3**), as determined by single crystal X-ray diffraction. Ellipsoids are shown at 50% probability level. Counterions, solvent molecules and partial hydrogen atoms are omitted for clarity. Color scheme: C, dark gray; N, blue; B, pink; Fe, orange; H gray. Selected bond distances (Å) and angles (deg): Fe1-C5 2.133(2), Fe1-C12 2.125(2), Fe1-N5 2.0492(18), Fe1-N6 2.0242(18); C5-Fe1-C12 95.47(8), N5-Fe1-N6 128.78(8), C5-Fe1-N5 110.24(7), C12-Fe1-N6 98.10(8).

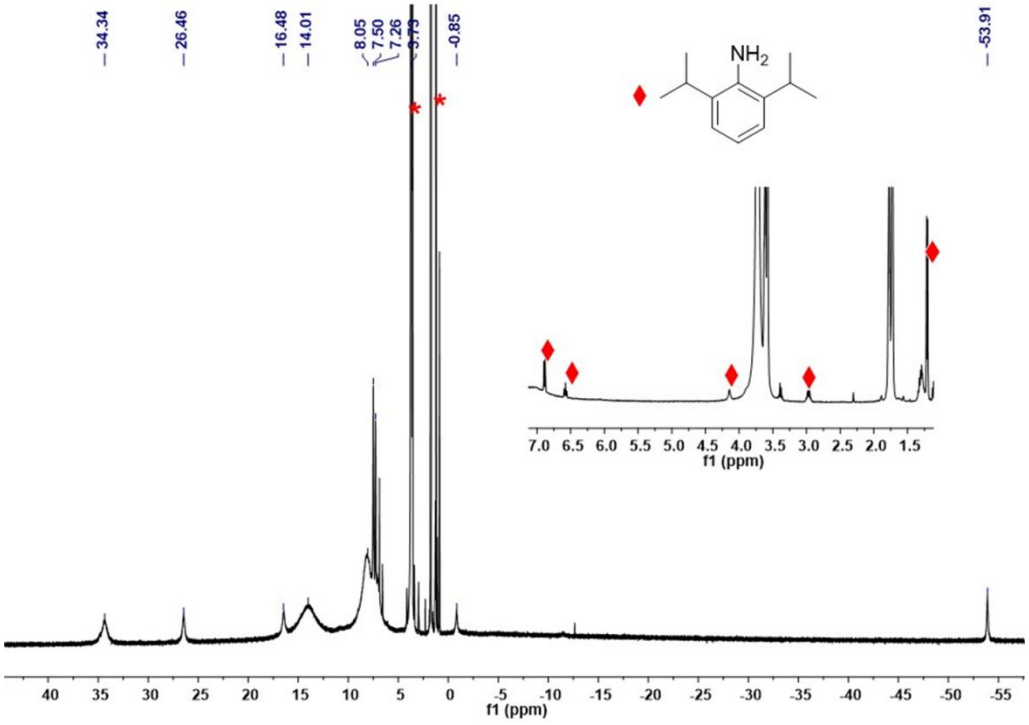


**Figure S10.** $^1H$ NMR spectrum (400 MHz, 25 °C, $d_8$-THF (*)) of $[Ph_2B(^tBuIm)_2Fe(NHDipp)_2][K(18\text{-}C\text{-}6)THF_2]$ (**3**).

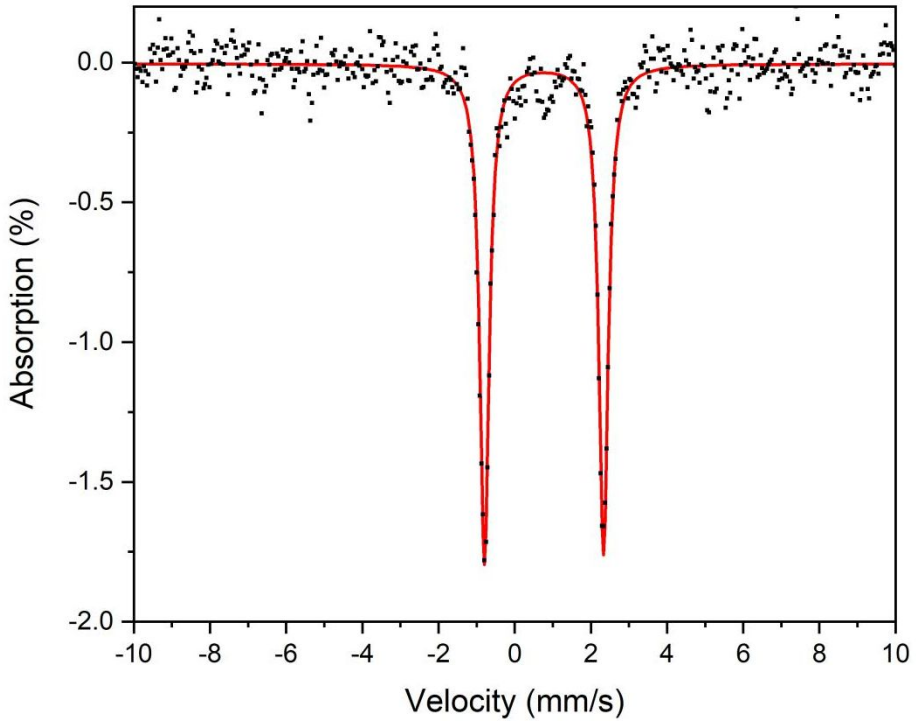


**Figure S11.** Zero-field $^{57}$Fe Mössbauer spectrum of $[Ph_2B(^tBuIm)_2Fe(NHDipp)_2][K(18\text{-}C\text{-}6)THF_2]$ (**3**) measured at 80 K. Parameters: $\delta = 0.76$ mm/s, $\Delta E_Q = 3.13$ mm/s.

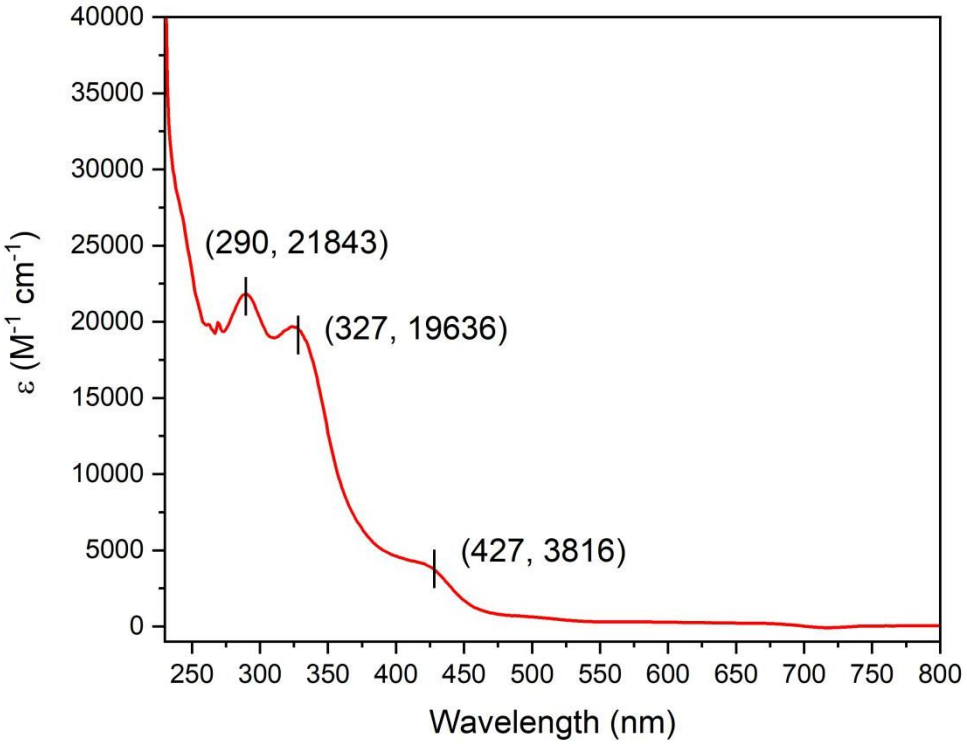


**Figure S12.** UV-vis spectrum of $[Ph_2B(^tBuIm)_2Fe(NHDipp)_2][K(18\text{-}C\text{-}6)THF_2]$ (**3**) measured at 25 °C in THF.

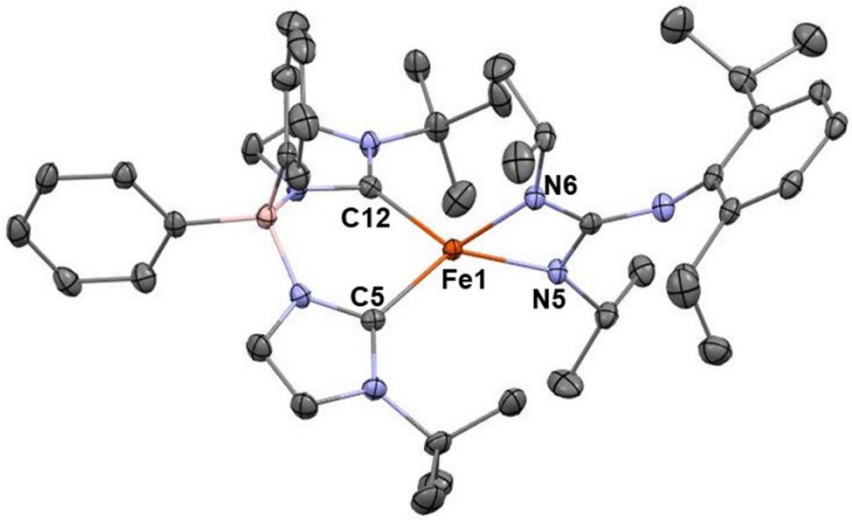


**Figure S13.** Molecular structure of $[Ph_2B(^tBuIm)_2Fe(^iPrN)_2CNDipp][K(18\text{-}C\text{-}6)THF_2]$ (**4**), as determined by single crystal X-ray diffraction. Ellipsoids are shown at 50% probability level. Hydrogen atoms, counterions and solvent molecules are omitted for clarity. Color scheme: C, dark gray; N, blue; B, pink; Fe, orange. Selected bond distances (Å) and angles (deg): Fe1-C5 2.126(2), Fe-C12 2.119(2), Fe1-N5 2.0307(19), Fe1-N6 1.998(2); C5-Fe1-C12 94.55(9), N5-Fe1-N6 66.55(8), C5-Fe1-N5 131.18(8), C12-Fe1-N6 120.79(8).

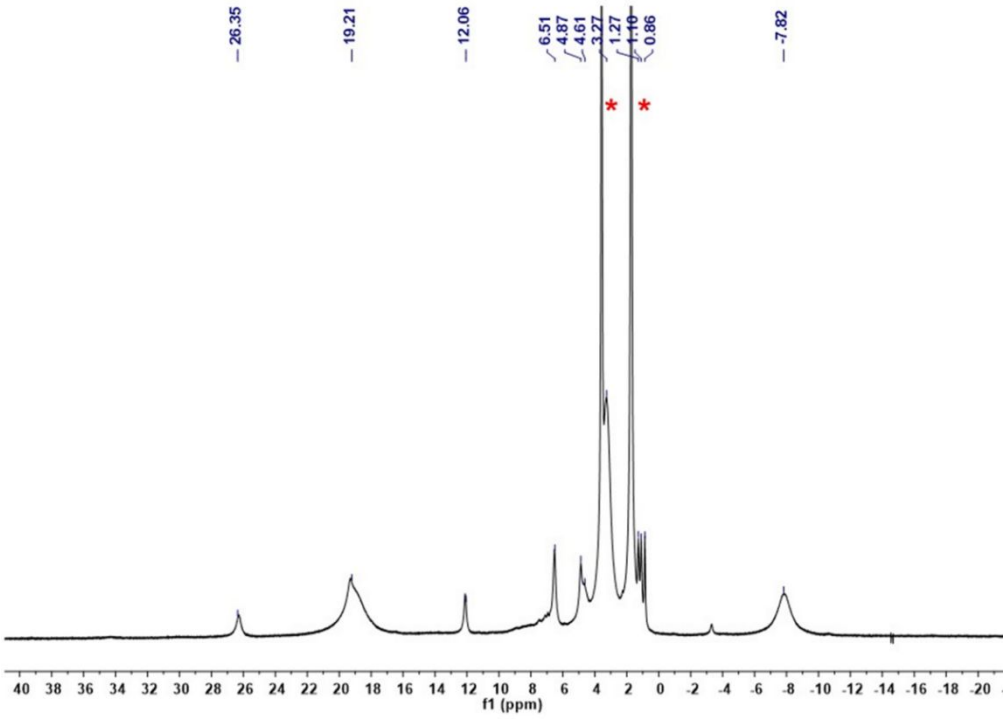


**Figure S14.** $^1H$ NMR spectrum (400 MHz, 25 °C, $d_8$-THF (*)) of $[Ph_2B(^tBuIm)_2Fe(^iPrN)_2CNDipp][K(18\text{-}C\text{-}6)THF_2]$ (**4**).

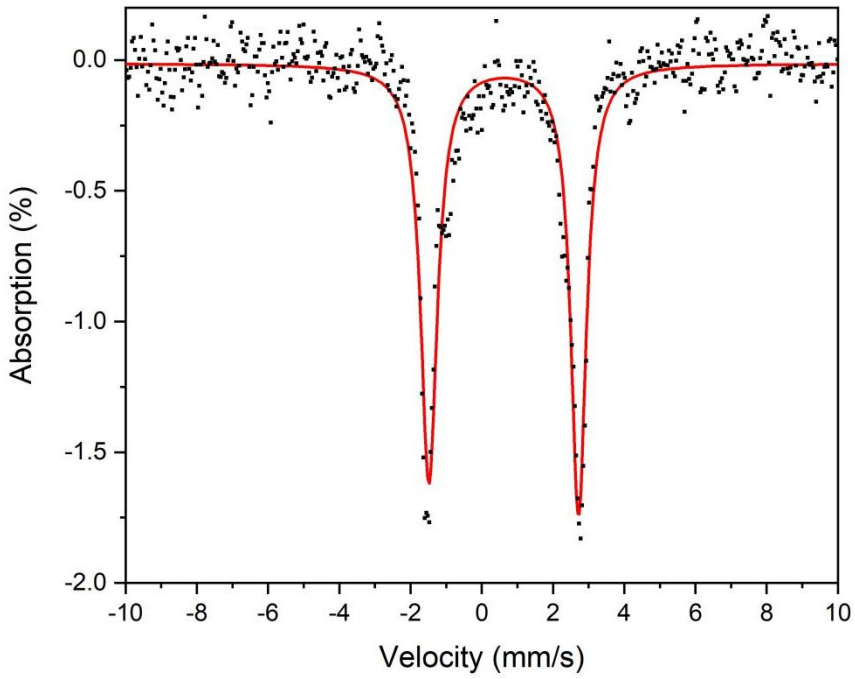


**Figure S15.** Zero-field $^{57}$Fe Mössbauer spectrum of [$Ph_2B(^tBuIm)_2Fe(^iPrN)_2CNDipp$][K(18-C-6)$THF_2$] (**4**) measured at 80 K. Parameters: $\delta$ = 0.62 mm/s, $\Delta E_Q$ = 4.20 mm/s.

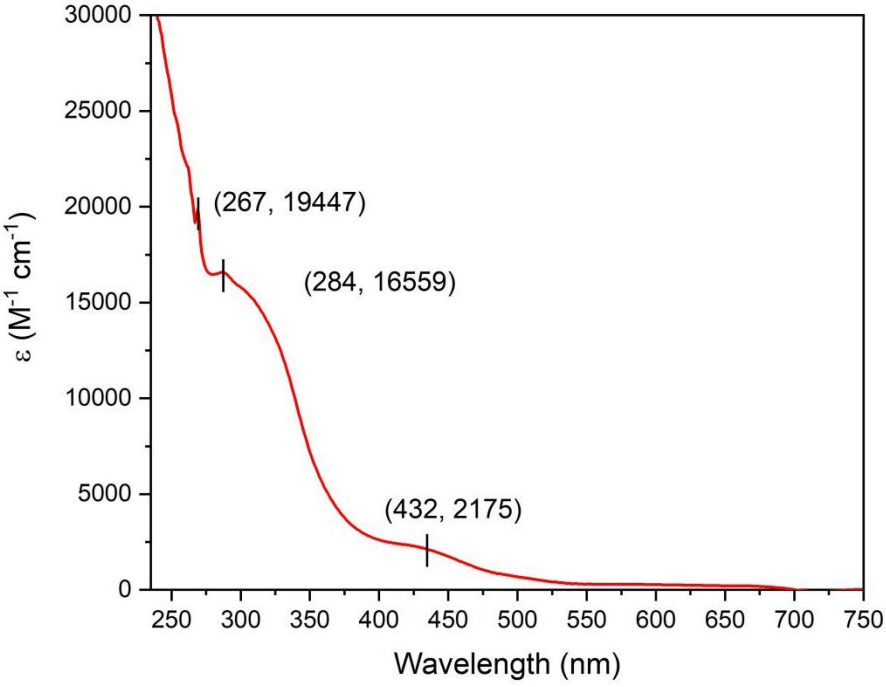


**Figure S16.** UV-vis spectrum of [$Ph_2B(^tBuIm)_2Fe(^iPrN)_2CNDipp$][K(18-C-6)$THF_2$] (**4**) measured at 25 °C in THF.

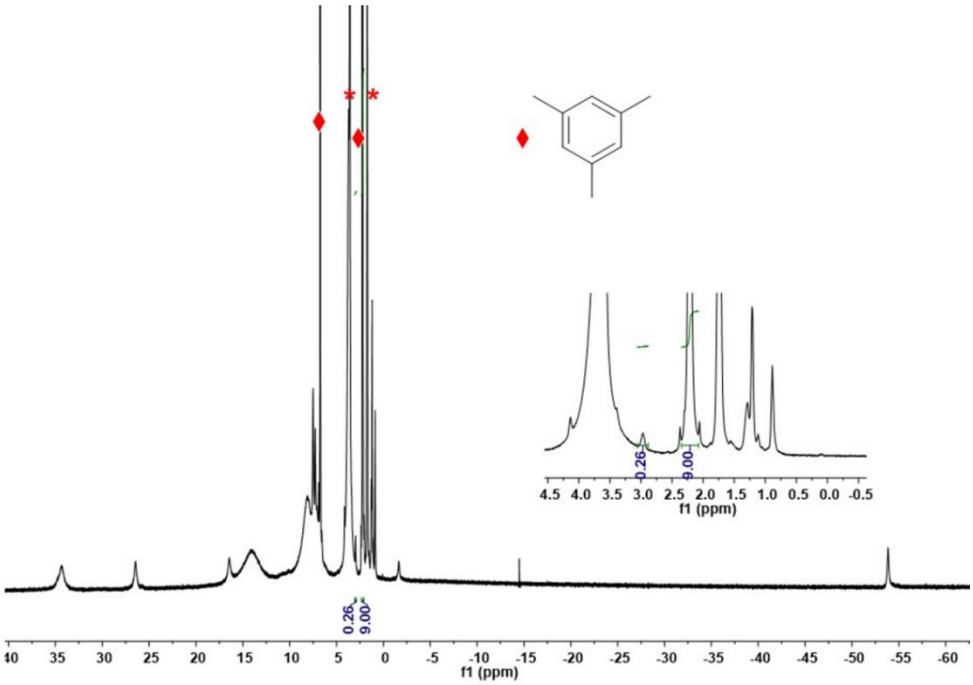


**Figure S17.** $^1$H NMR spectrum (400 MHz, 25 °C, $d_8$-THF (*)) of $[Ph_2B(^tBuIm)_2Fe(NHDipp)_2][K(18\text{-}C\text{-}6)THF_2]$ (**3**) in the presence of mesitylene.

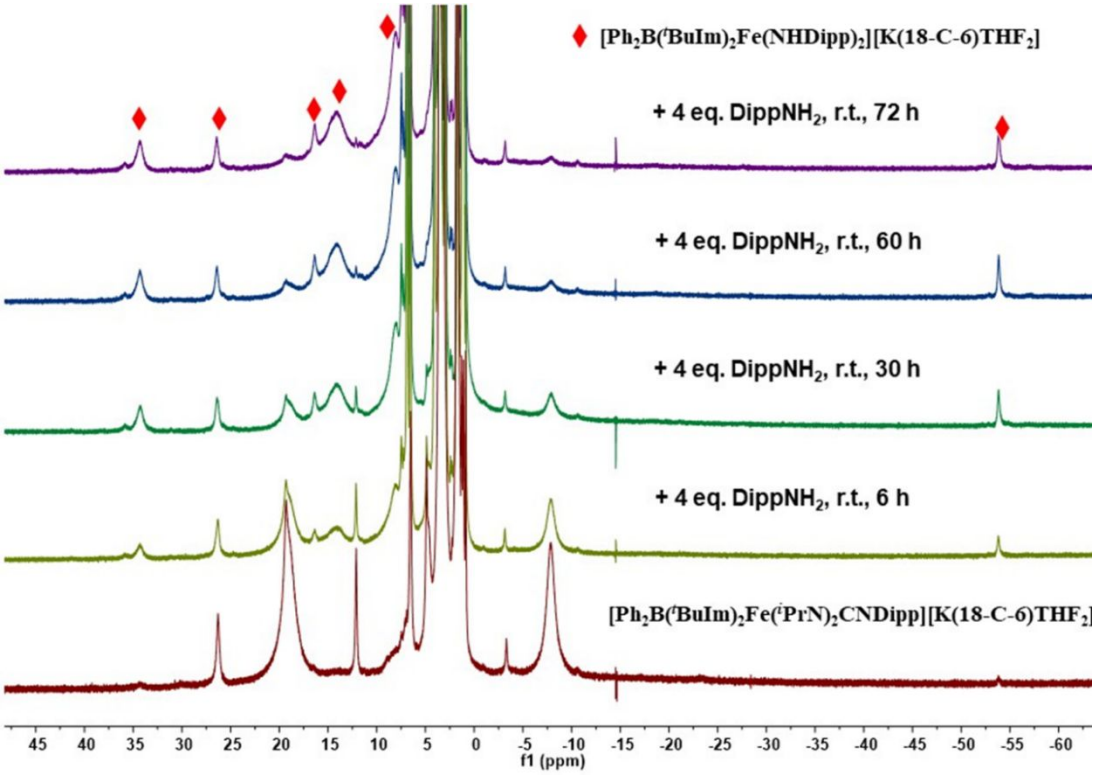


**Figure S18.** $^1$H NMR spectrum (400 MHz, 25 °C, $d_8$-THF) of the reaction of $[Ph_2B(^tBuIm)_2Fe(^iPrN)_2CNDipp][K(18\text{-}C\text{-}6)THF_2]$ (**4**) with 4 eq. $DippNH_2$.

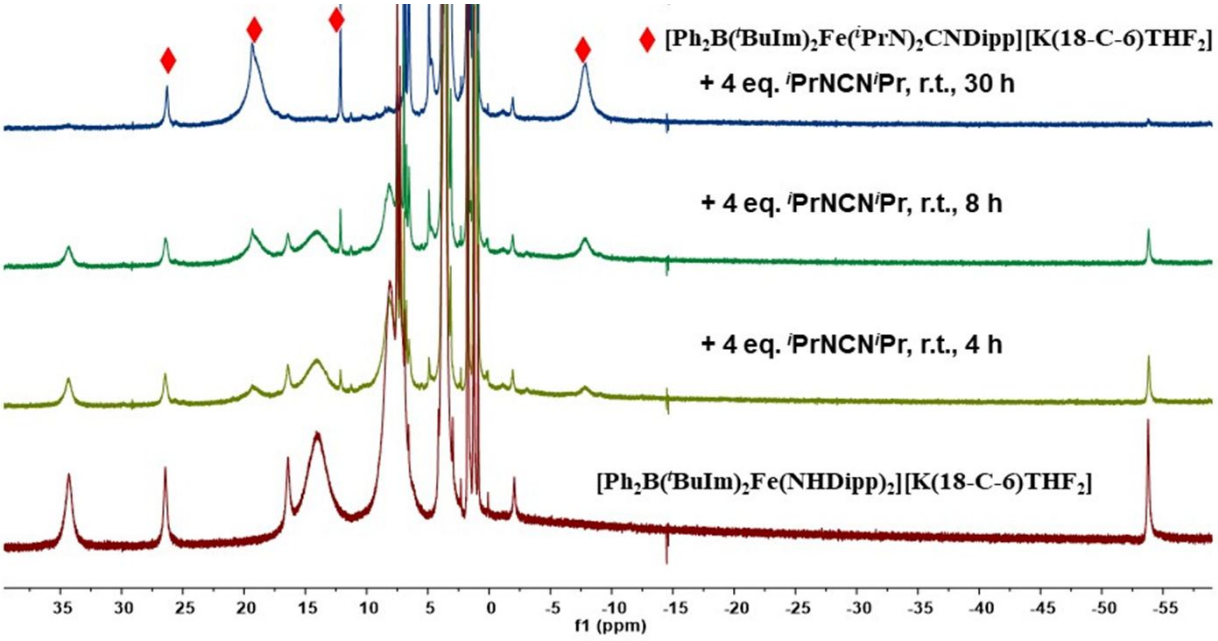


**Figure S19.** $^1$H NMR spectrum (400 MHz, 25 °C, $d_8$-THF) of the reaction of $[Ph_2B(^tBuIm)_2Fe(NHDipp)_2][K(18\text{-}C\text{-}6)THF_2]$ (**3**) with 4 eq. *N,N′*-Diisopropylcarbodiimide ($^i$PrNCN$^i$Pr).

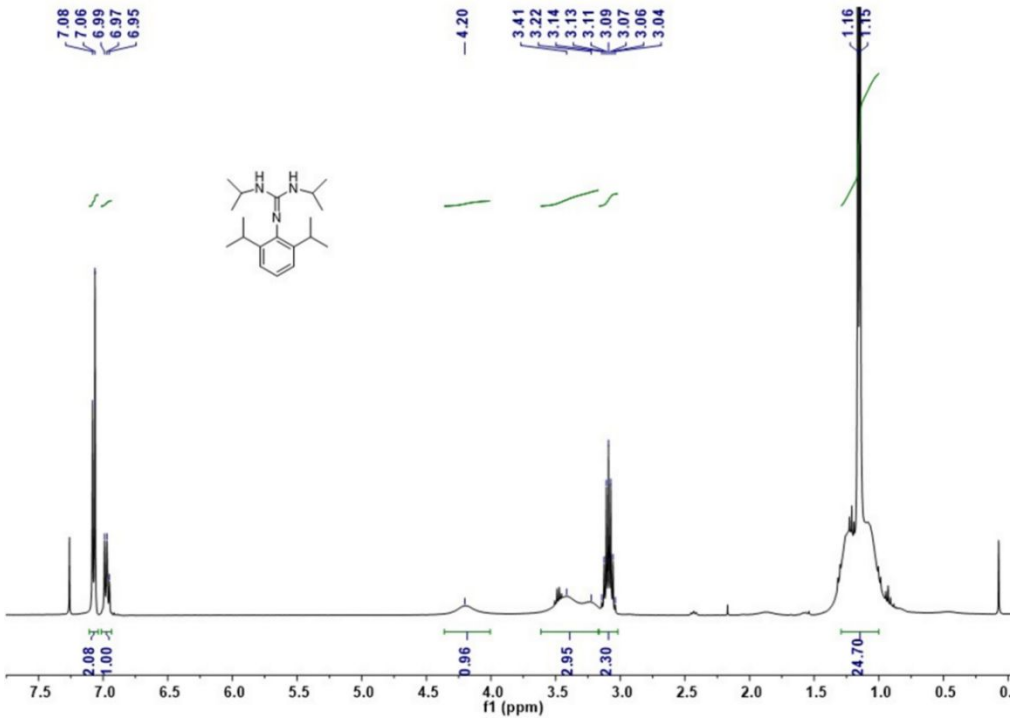


**Figure S20.** $^1$H NMR spectrum (400 MHz, 25 °C, $CDCl_3$) of *N*-2,6-diisopropylphenyl-*N′, N″*-diisopropylguanidine.

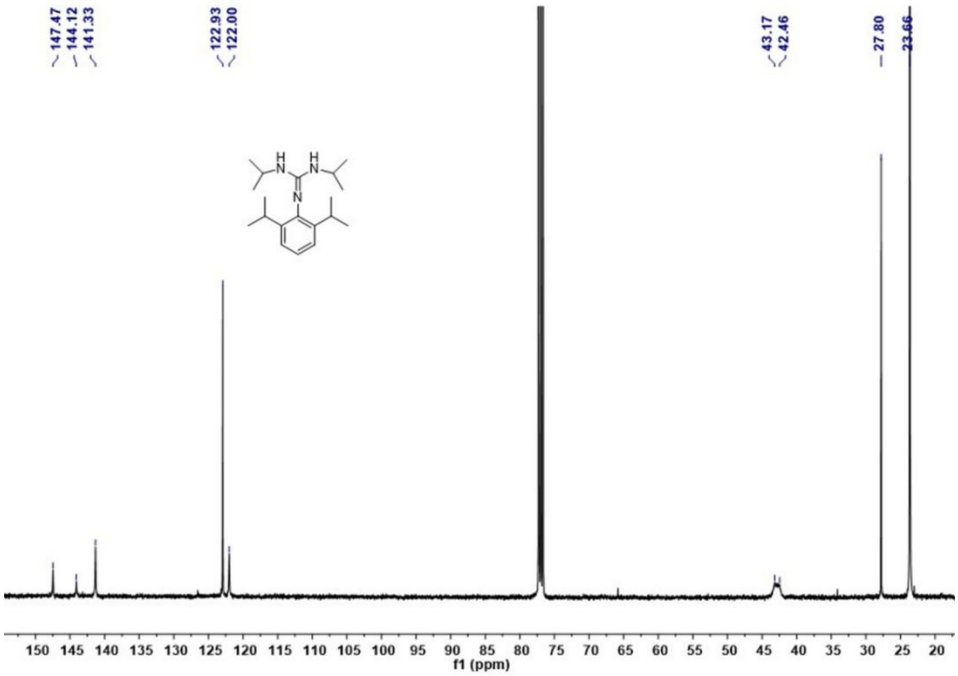


**Figure S21.** $^{13}C$ NMR spectrum (101 MHz, 25 °C, $CDCl_3$) of *N*-2,6-diisopropylphenyl-*N′, N″*-diisopropylguanidine.

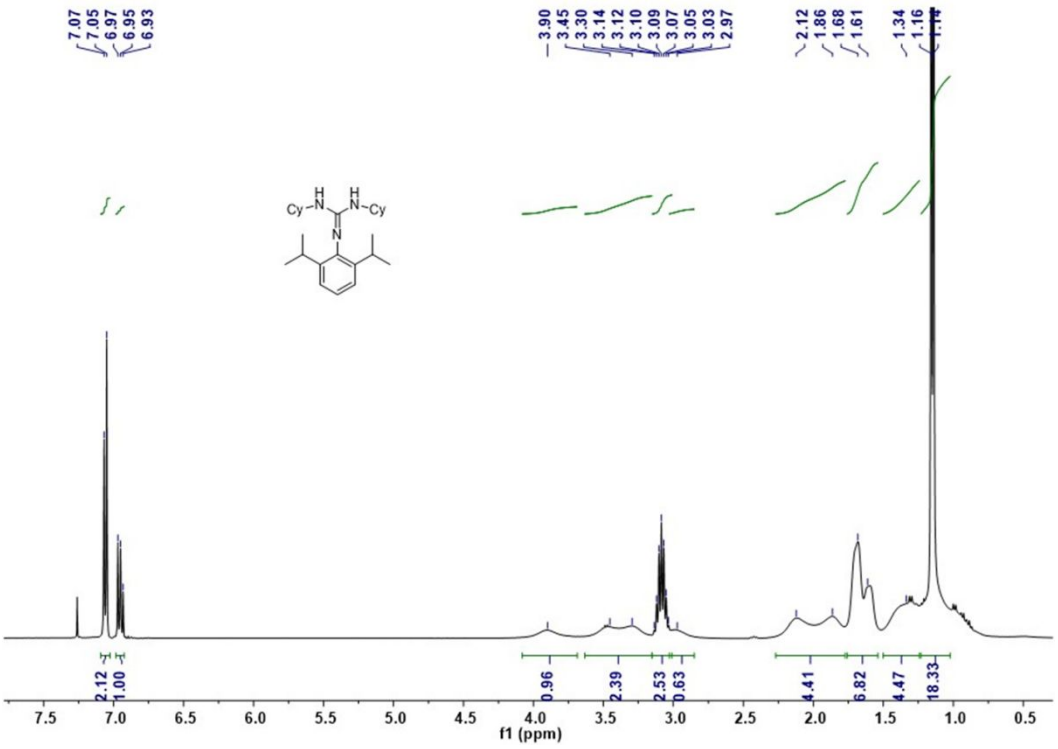


**Figure S22.** $^{1}H$ NMR spectrum (400 MHz, 25 °C, $CDCl_3$) of *N*-2,6-diisopropylphenyl-*N′, N″*-dicyclohexylguanidine.

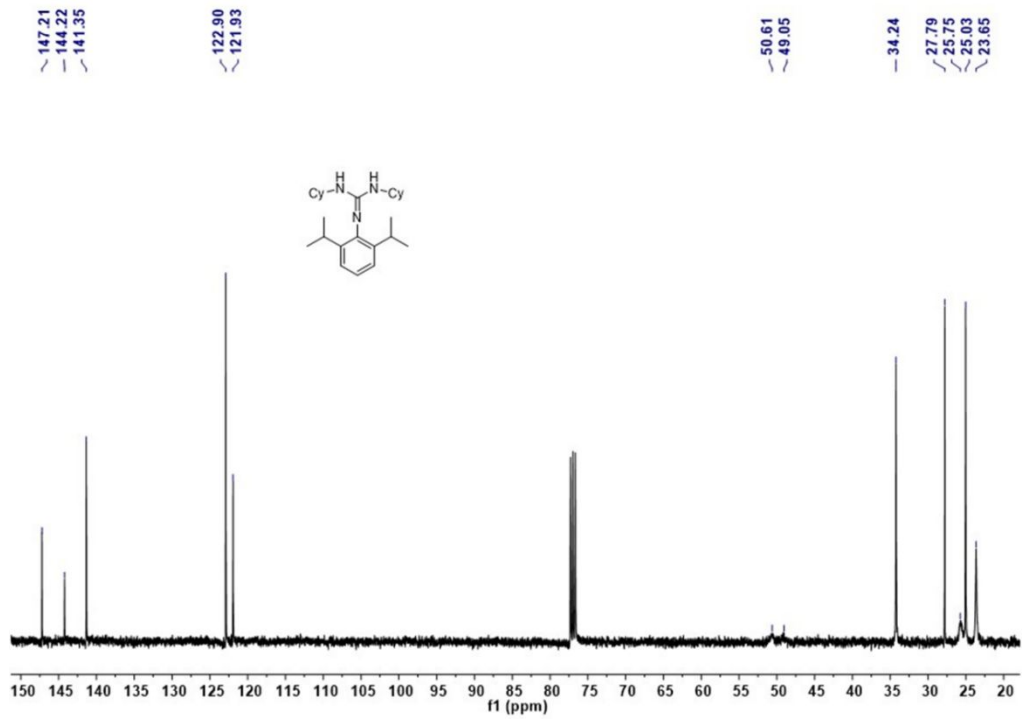


**Figure S23.** $^{13}C$ NMR spectrum (101 MHz, 25 °C, $CDCl_3$) of *N*-2,6-diisopropylphenyl-*N′, N″*-dicyclohexylguanidine.

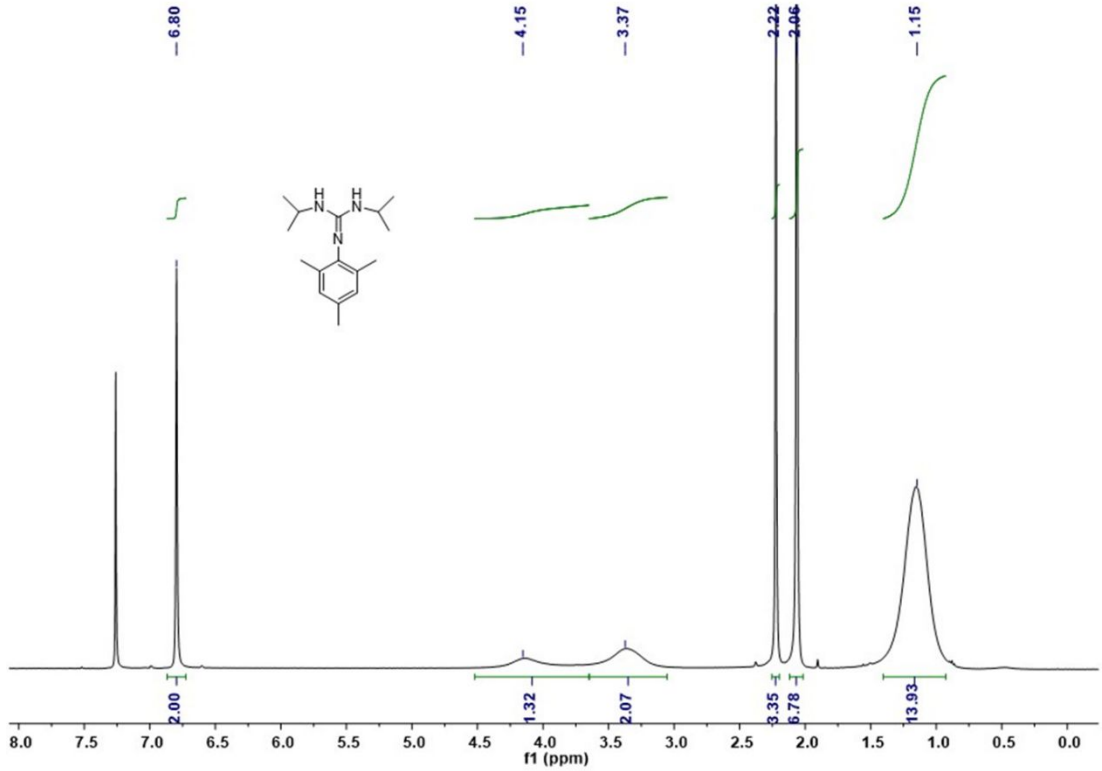


**Figure S24.** $^{1}H$ NMR spectrum (400 MHz, 25 °C, $CDCl_3$) of *N*-2,4,6-trimethylphenyl-*N′, N″*-diisopropylguanidine.

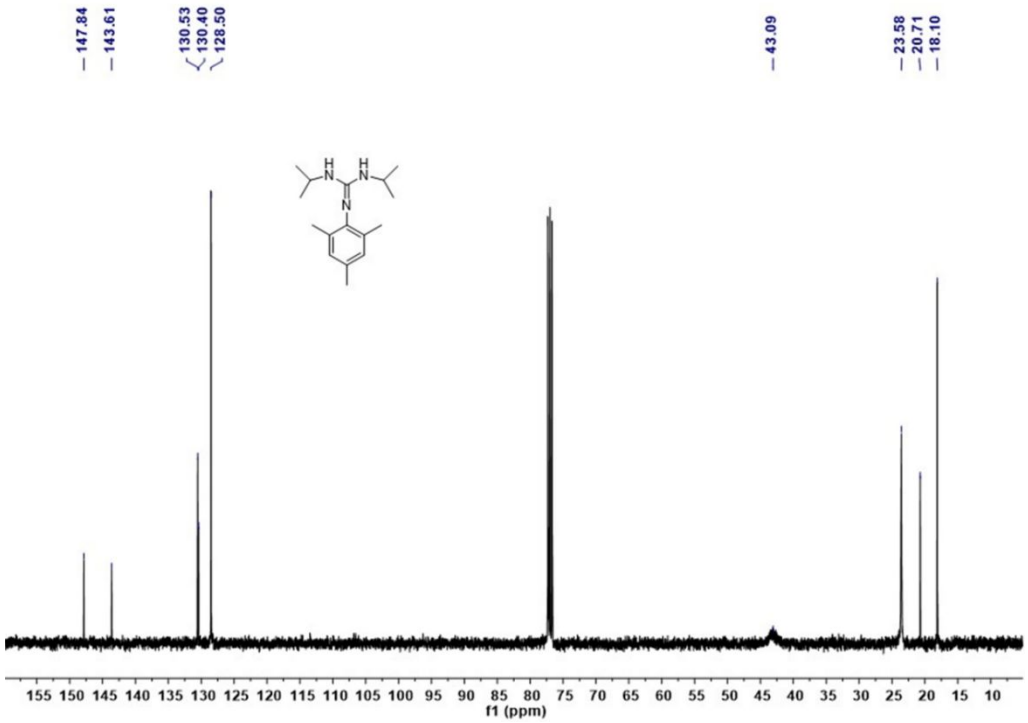


**Figure S25.** $^{13}C$ NMR spectrum (101 MHz, 25 °C, $CDCl_3$) of *N*-2,4,6-trimethylphenyl-*N′, N″*-diisopropylguanidine.

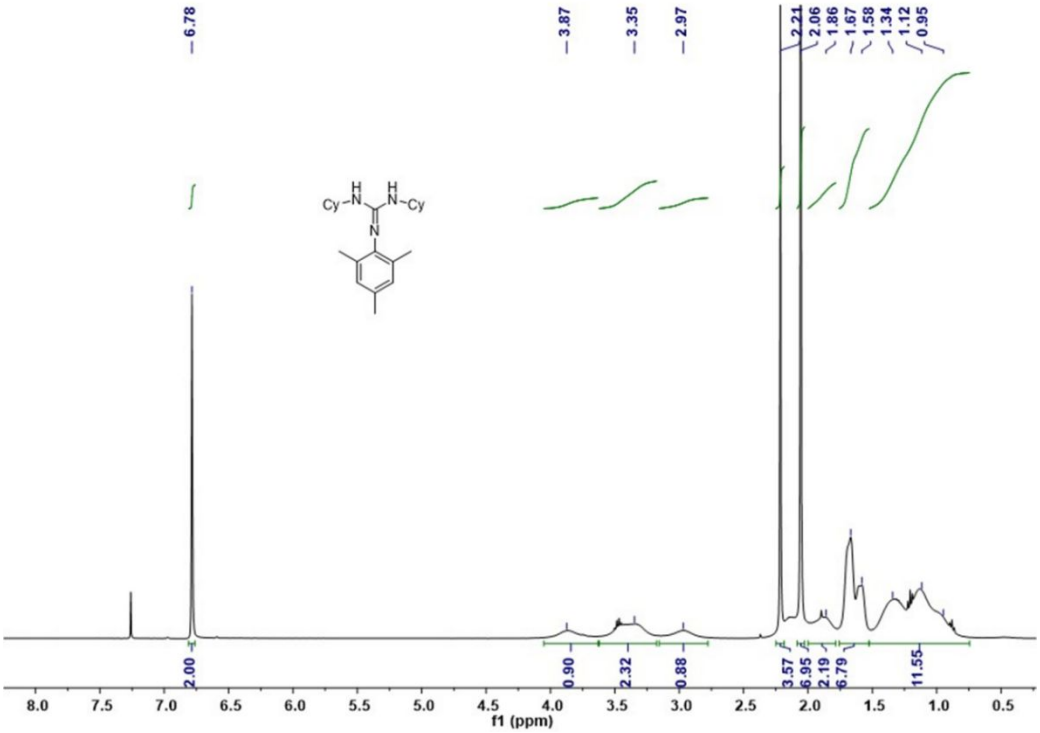


**Figure S26.** $^{1}H$ NMR spectrum (400 MHz, 25 °C, $CDCl_3$) of *N*-2,4,6-trimethylphenyl-*N′, N″*-dicyclohexylguanidine.

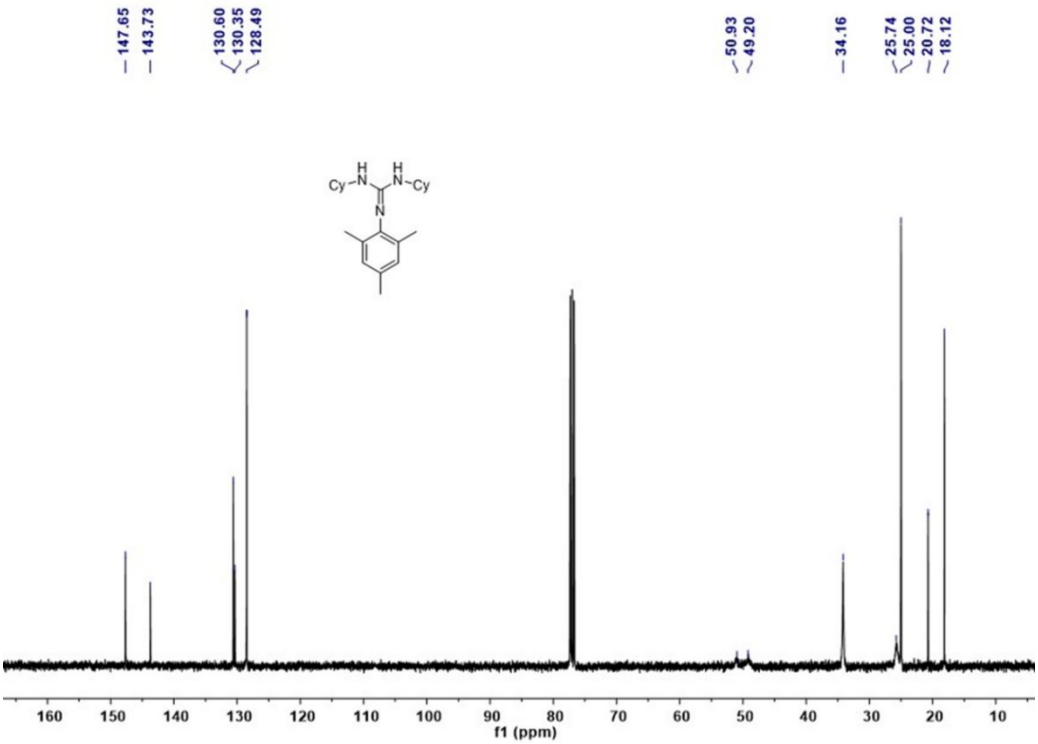


**Figure S27.** $^{13}C$ NMR spectrum (101 MHz, 25 °C, $CDCl_3$) of *N*-2,4,6-trimethylphenyl-*N′, N″*-dicyclohexylguanidine.

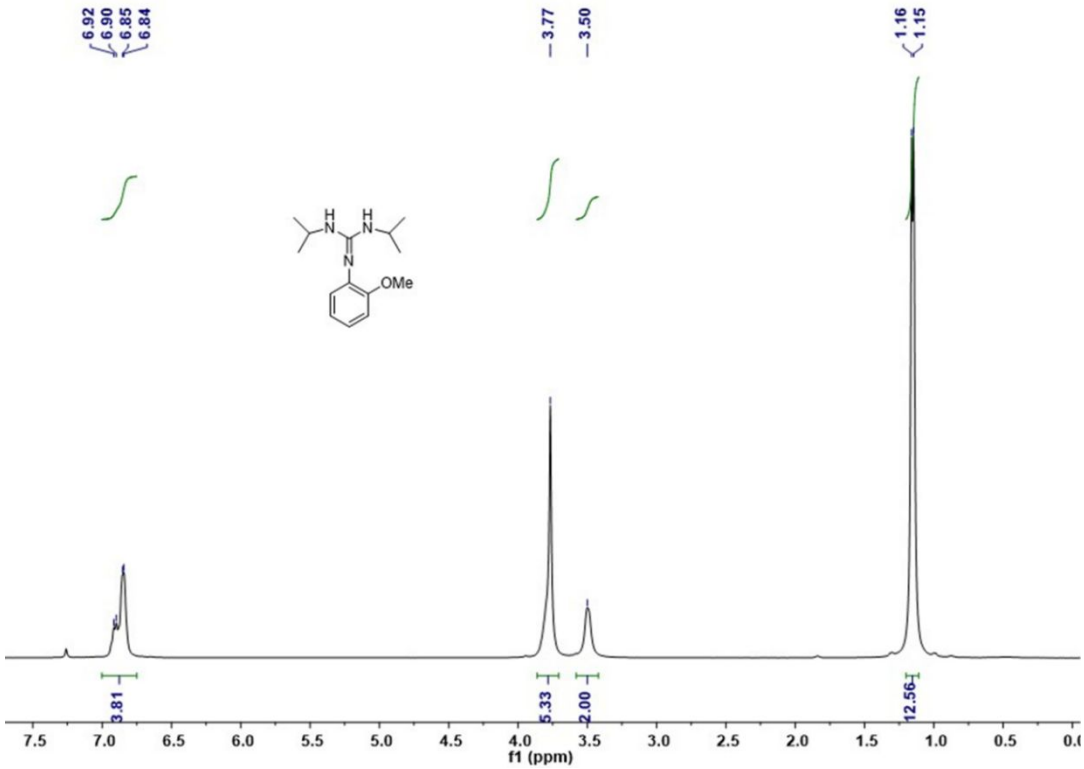


**Figure S28.** $^{1}H$ NMR spectrum (400 MHz, 25 °C, $CDCl_3$) of *N*-*o*-methoxyphenyl-*N′*, *N″*-diisopropylguanidine.

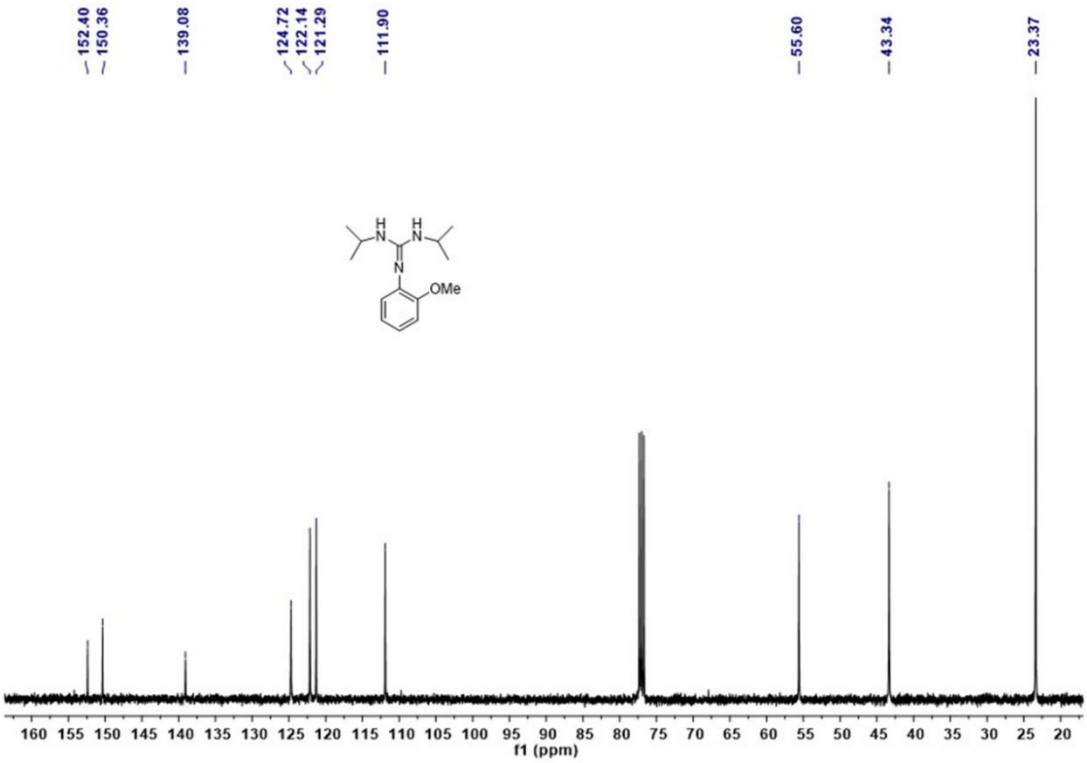


**Figure S29.** $^{13}C$ NMR spectrum (101 MHz, 25 °C, $CDCl_3$) of *N*-*o*-methoxyphenyl-*N′*, *N″*-diisopropylguanidine.

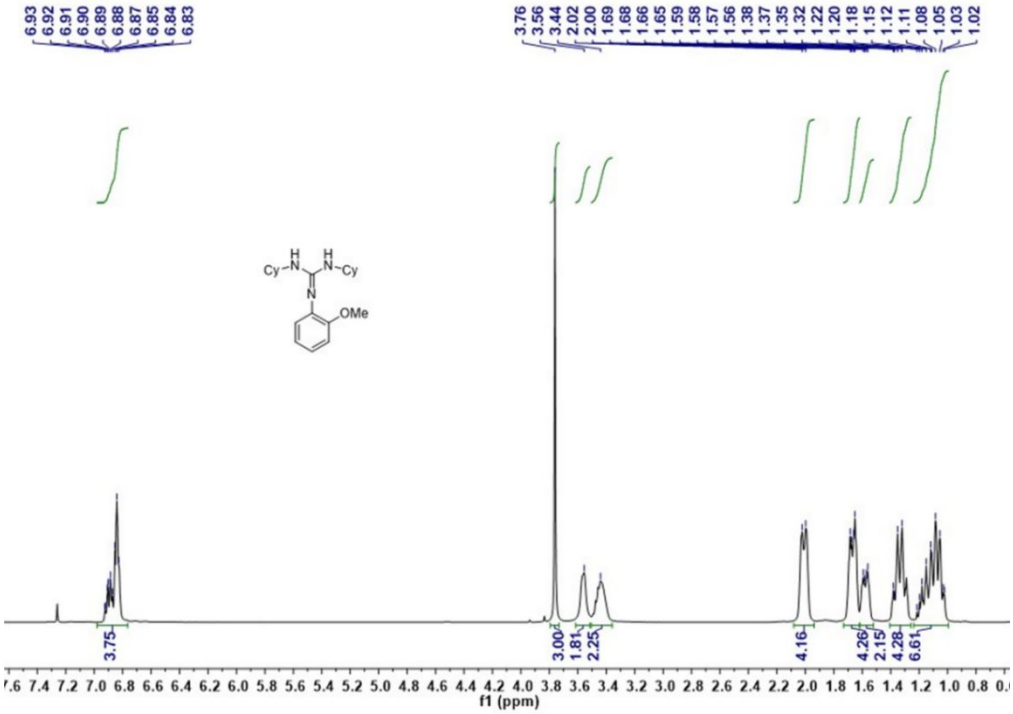


**Figure S30.** $^{1}H$ NMR spectrum (400 MHz, 25 °C, $CDCl_3$) of *N*-*o*-methoxyphenyl-*N′, N″*-dicyclohexylguanidine.

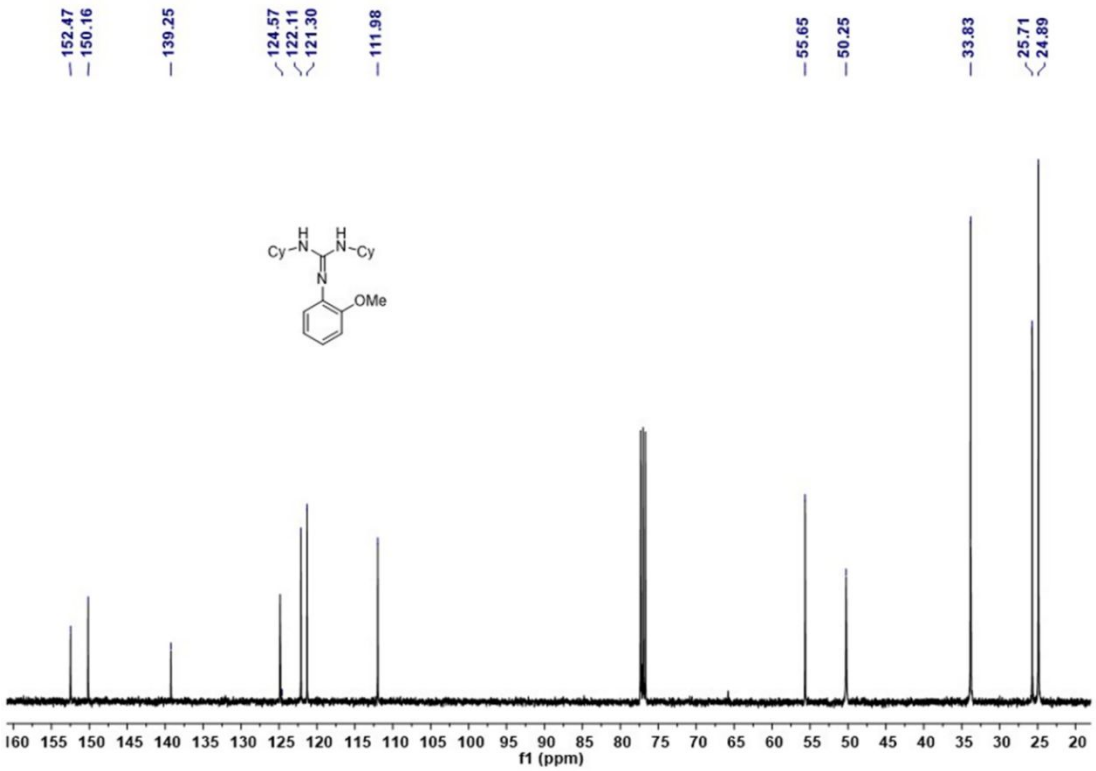


**Figure S31.** $^{13}C$ NMR spectrum (101 MHz, 25 °C, $CDCl_3$) of *N*-*o*-methoxyphenyl-*N′, N″*-dicyclohexylguanidine.

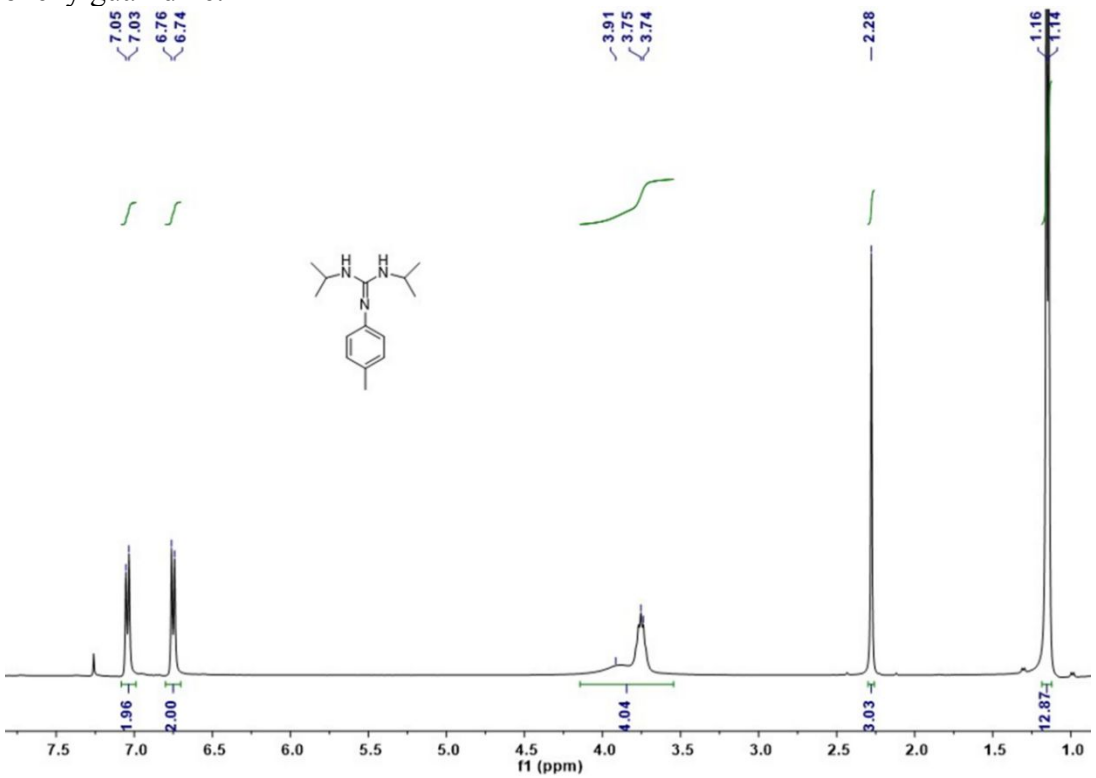


**Figure S32.** $^{1}H$ NMR spectrum (400 MHz, 25 °C, $CDCl_3$) of *N*-*p*-methylphenyl-*N′, N″*-diisopropylguanidine.

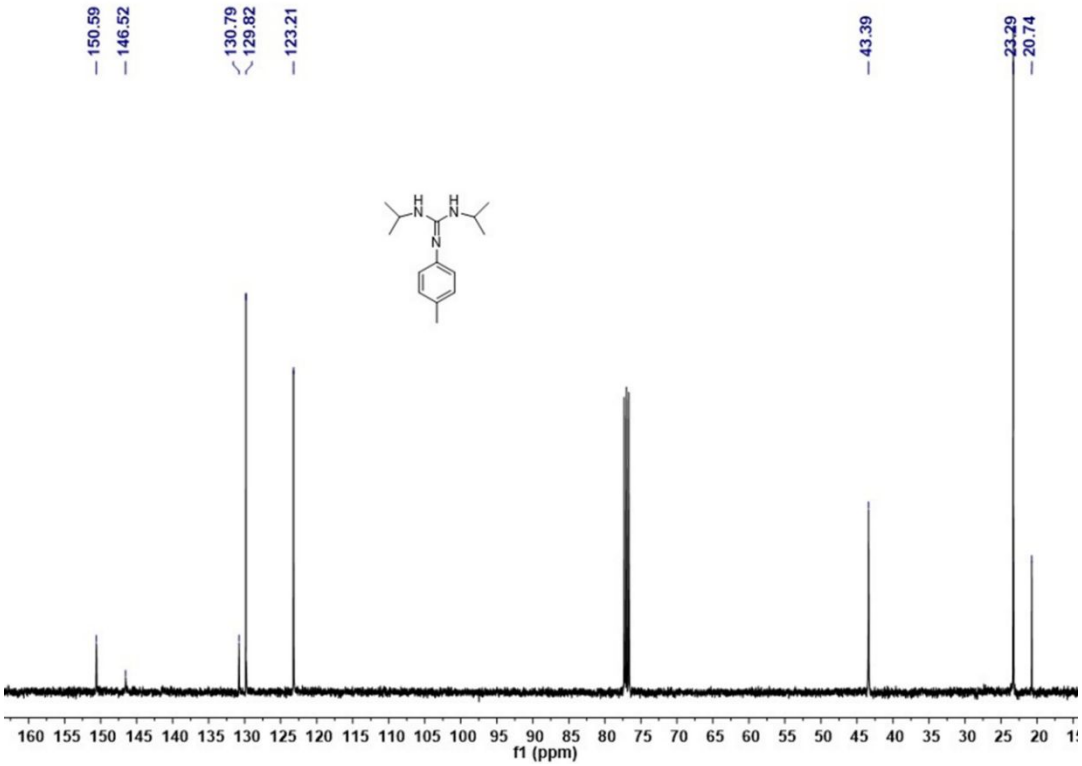


**Figure S33.** $^{13}C$ NMR spectrum (101 MHz, 25 °C, $CDCl_3$) of *N*-*p*-methylphenyl-*N′, N″*-diisopropylguanidine.

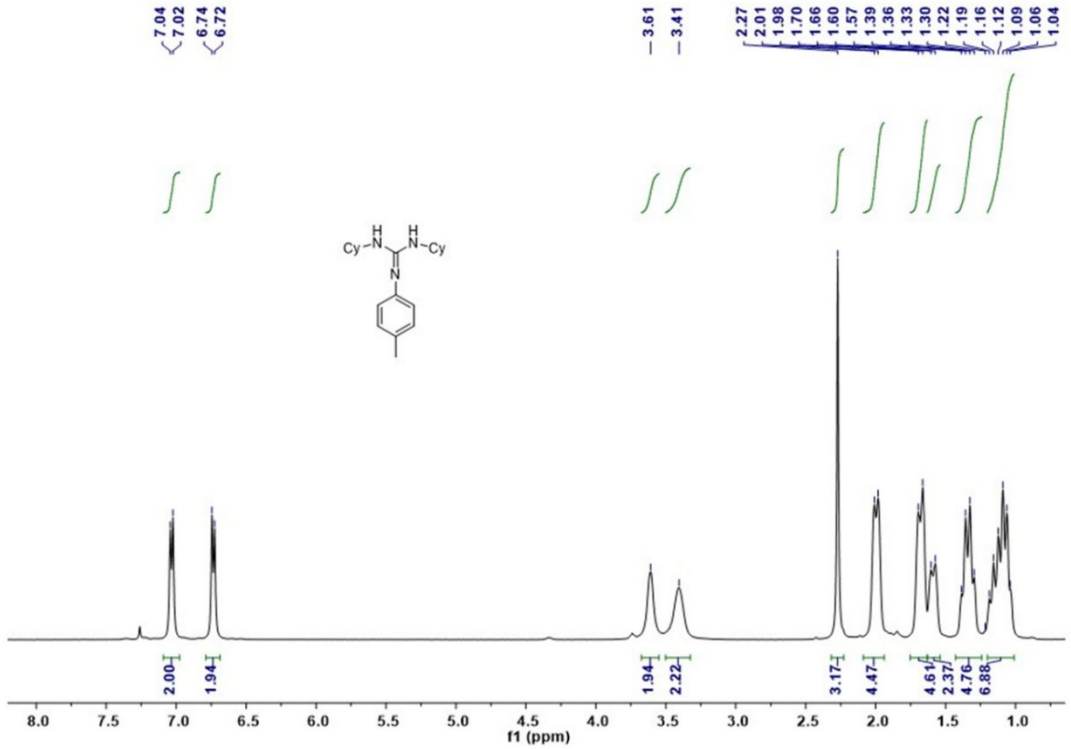


**Figure S34.** $^{1}H$ NMR spectrum (400 MHz, 25 °C, $CDCl_3$) of *N*-*p*-methylphenyl-*N′, N″*-dicyclohexylguanidine.

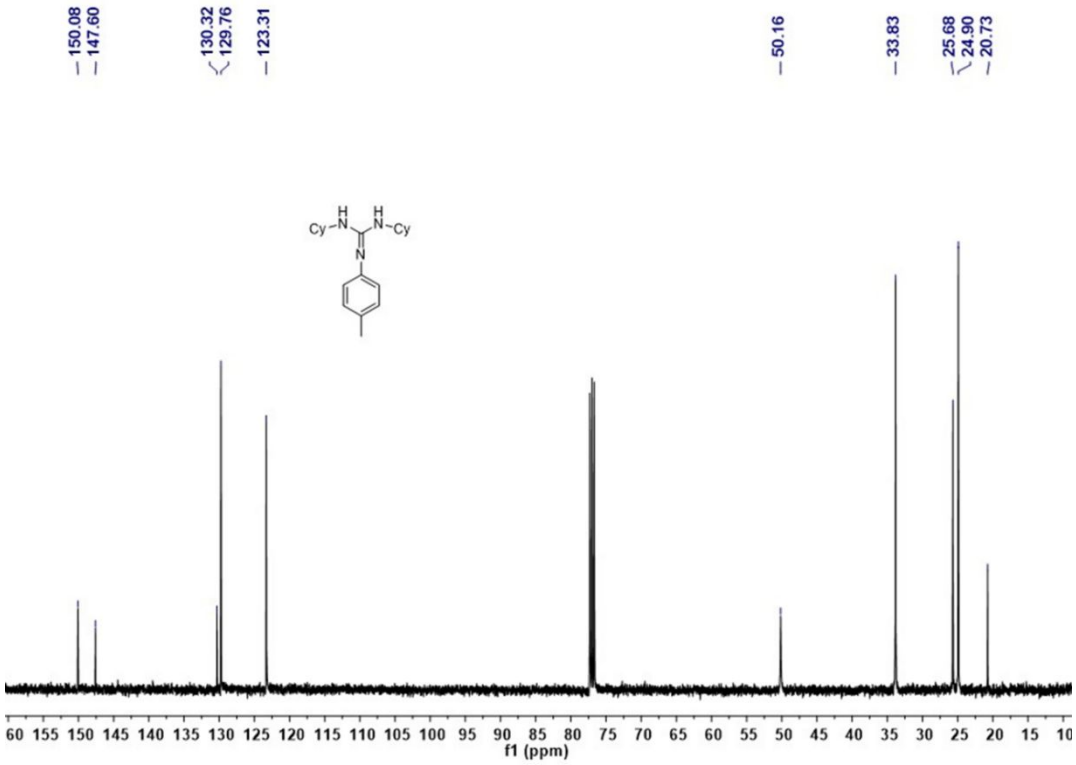


**Figure S35.** $^{13}C$ NMR spectrum (101 MHz, 25 °C, $CDCl_3$) of *N*-*p*-methylphenyl-*N′, N″*-dicyclohexylguanidine.

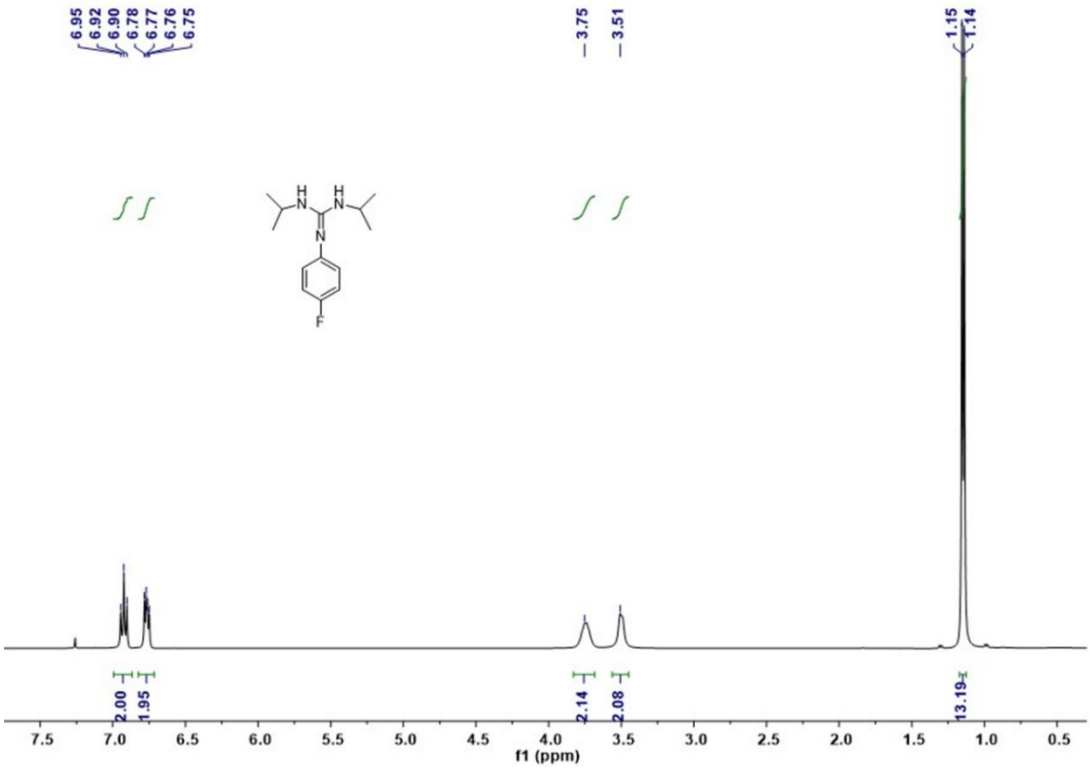


**Figure S36.** $^{1}H$ NMR spectrum (400 MHz, 25 °C, $CDCl_3$) of *N*-*p*-flurophenyl-*N′, N″*-diisopropylguanidine.

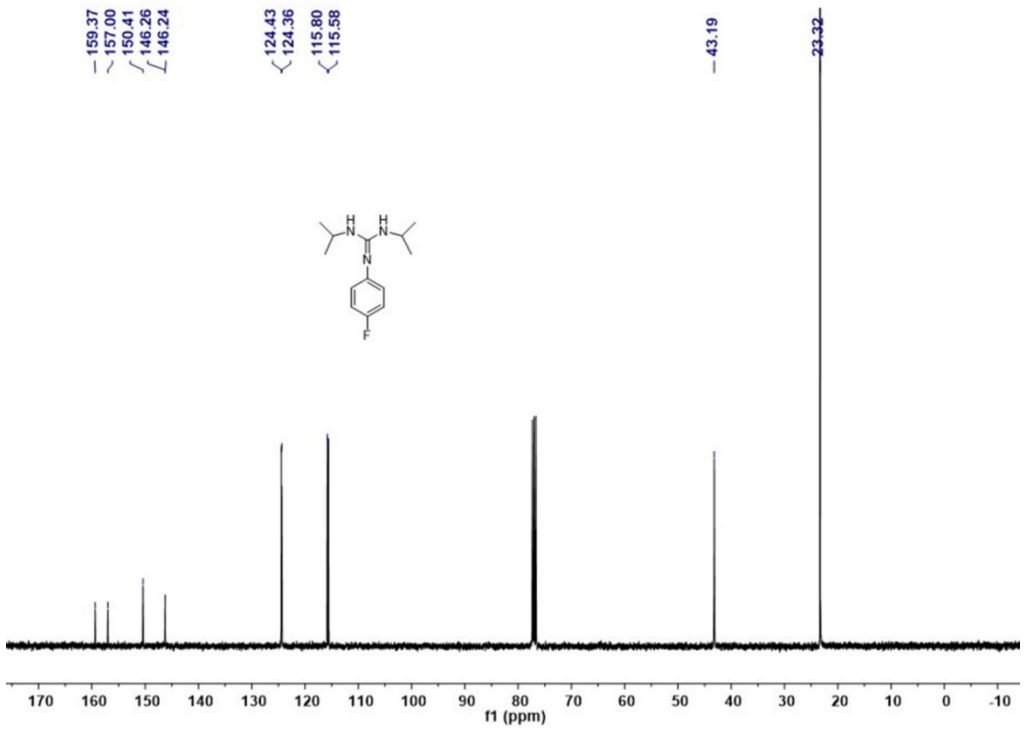


**Figure S37.** $^{13}C$ NMR spectrum (101 MHz, 25 °C, $CDCl_3$) of *N*-*p*-flurophenyl-*N′, N″*-diisopropylguanidine.

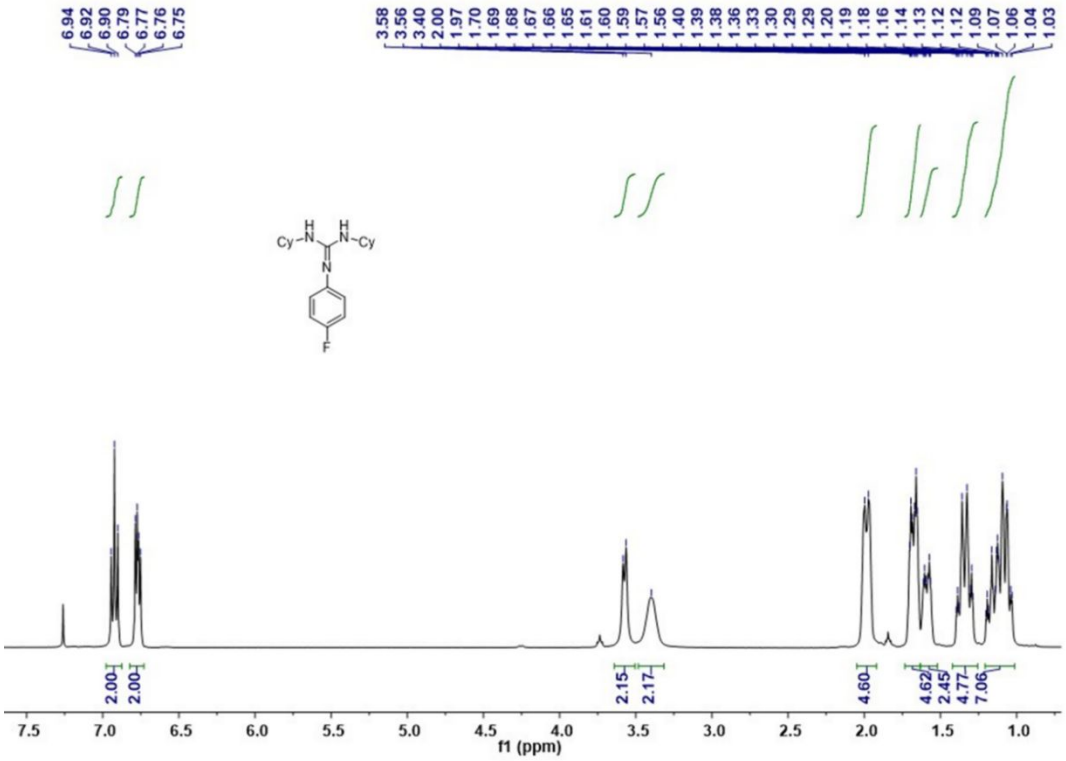


**Figure S38.** $^{1}H$ NMR spectrum (400 MHz, 25 °C, $CDCl_3$) of *N*-*p*-flurophenyl-*N′, N″*-dicyclohexylguanidine.

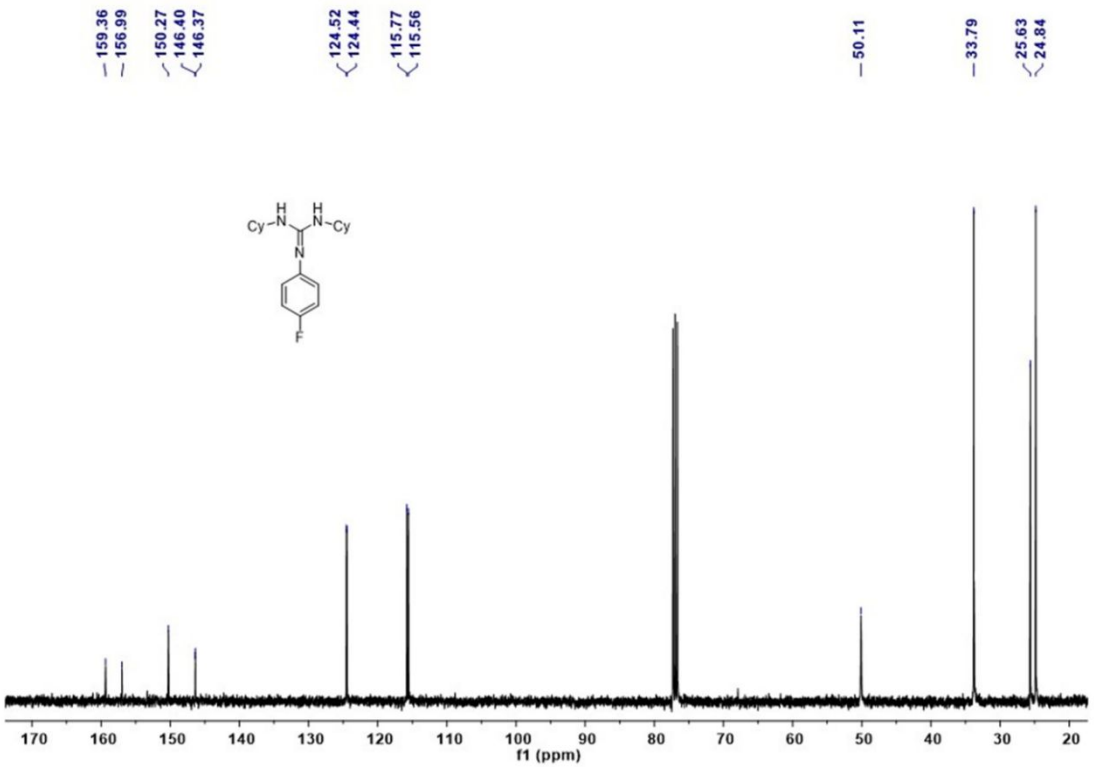


**Figure S39.** $^{13}C$ NMR spectrum (101 MHz, 25 °C, $CDCl_3$) of *N*-*p*-flurophenyl-*N′, N″*-dicyclohexylguanidine.

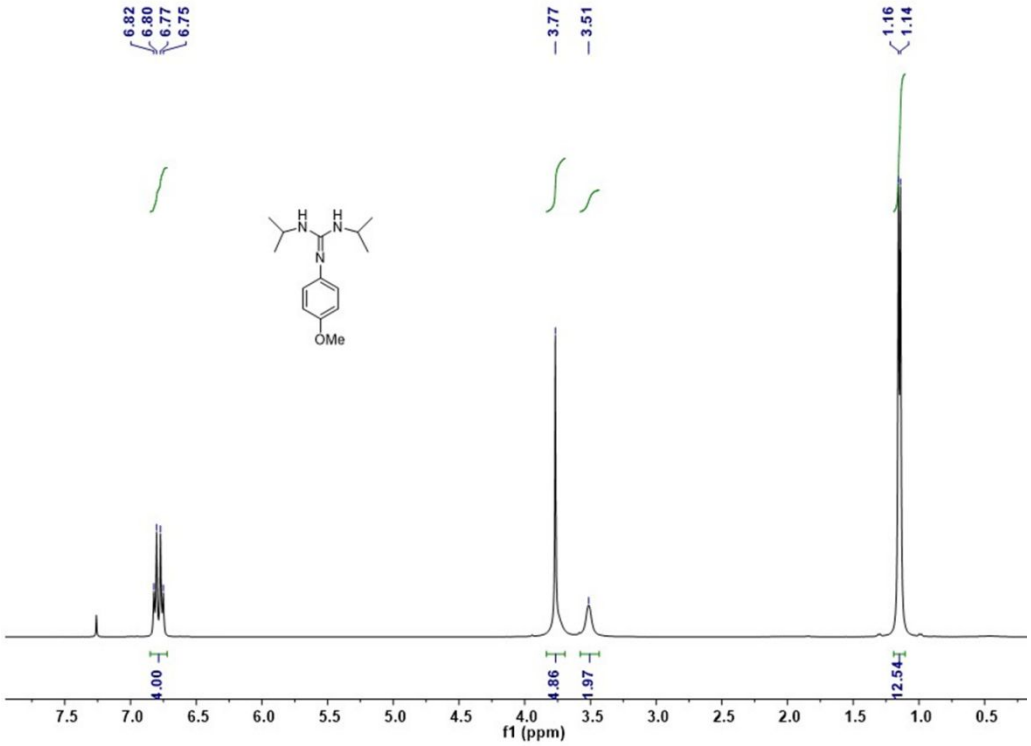


**Figure S40.** $^{1}H$ NMR spectrum (400 MHz, 25 °C, $CDCl_3$) of *N*-*p*-methoxyphenyl-*N′, N″*-diisopropylguanidine.

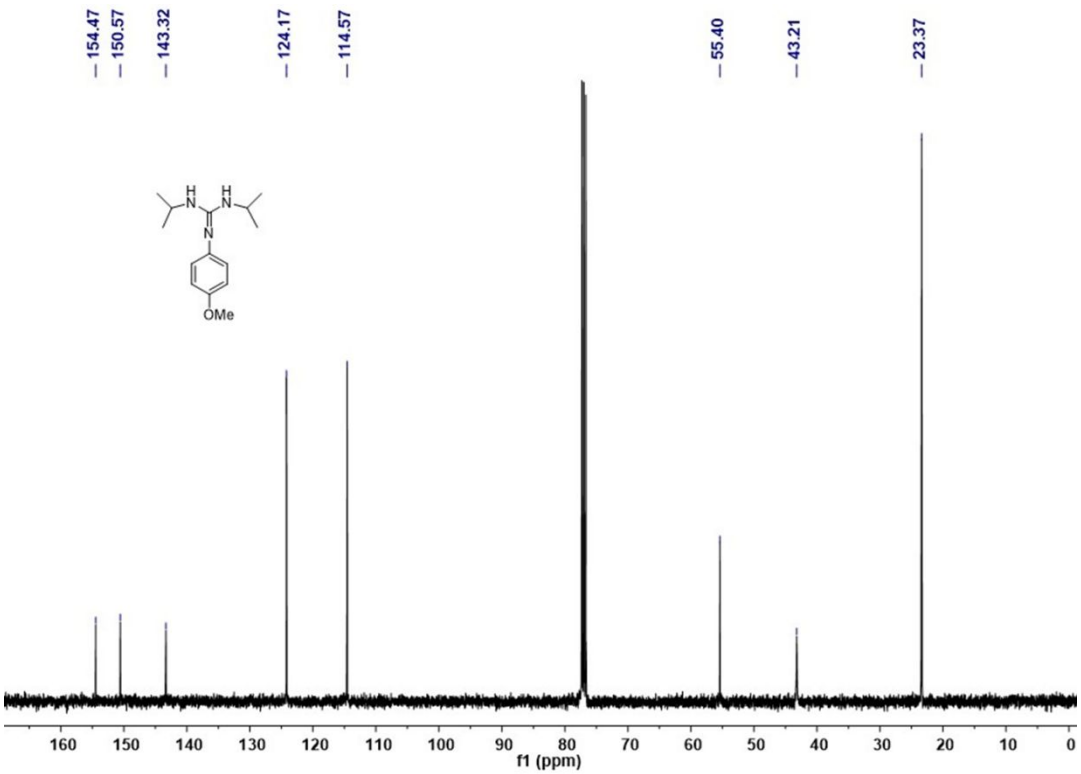


**Figure S41.** $^{13}C$ NMR spectrum (101 MHz, 25 °C, $CDCl_3$) of *N*-*p*-methoxyphenyl-*N′, N″*-diisopropylguanidine.

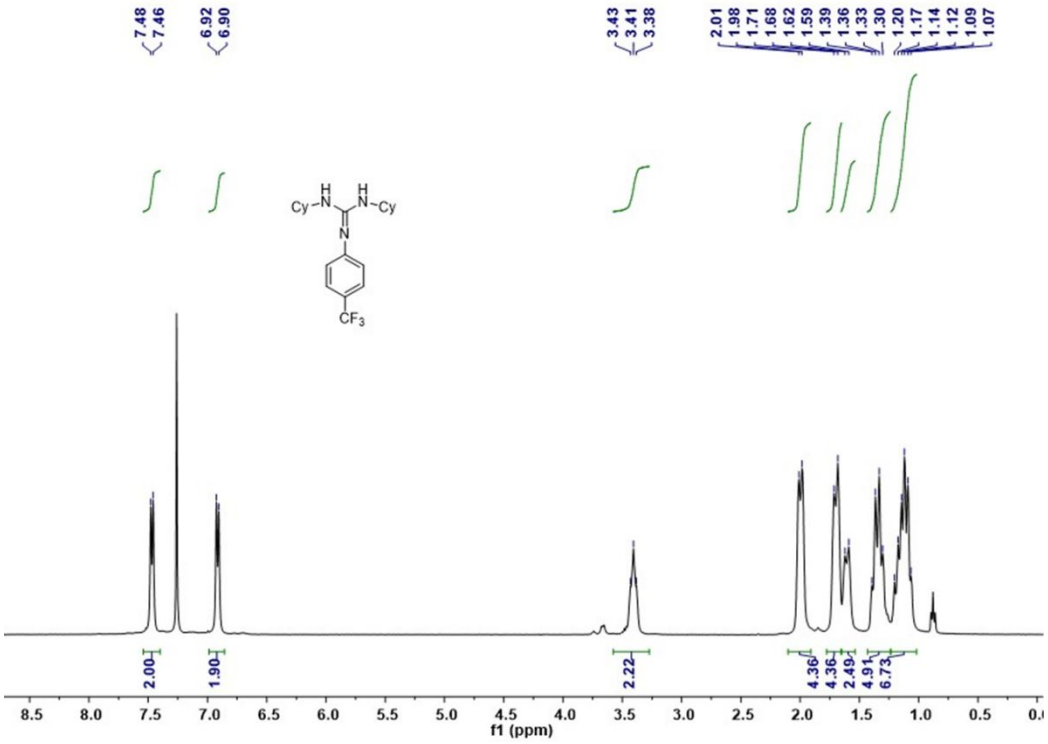


**Figure S42.** $^{1}H$ NMR spectrum (400 MHz, 25 °C, $CDCl_3$) of *N*-*p*-trifluoromethylphenyl-*N′, N″*-dicyclohexylguanidine.

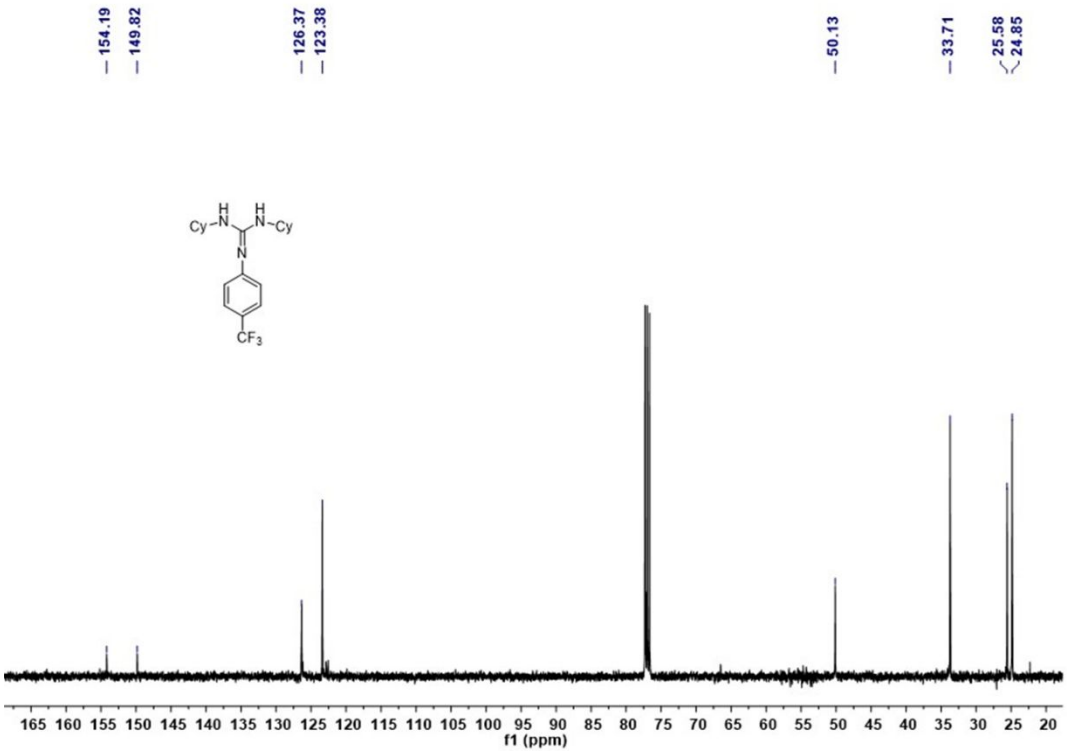


**Figure S43.** $^{13}C$ NMR spectrum (101 MHz, 25 °C, $CDCl_3$) of *N*-*p*-trifluoromethylphenyl-*N′, N″*-dicyclohexylguanidine.

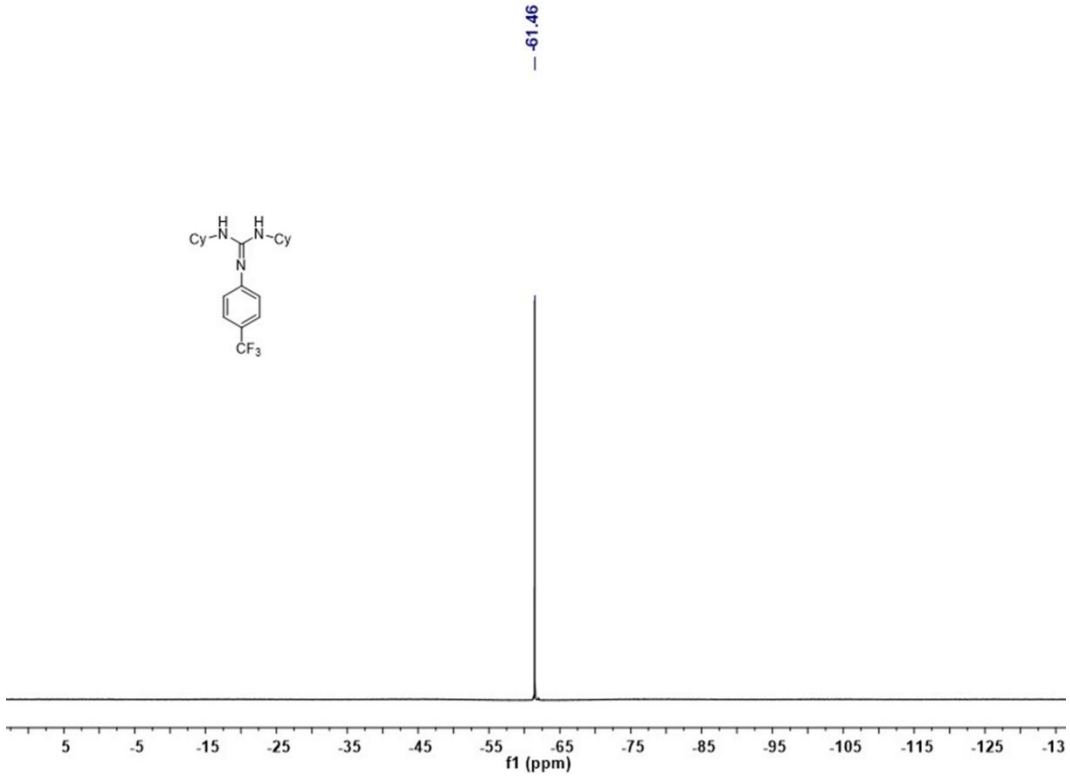


**Figure S44.** $^{19}F$ NMR spectrum (376 MHz, 25 °C, $CDCl_3$) of *N*-*p*-trifluoromethylphenyl-*N′, N″*-dicyclohexylguanidine.

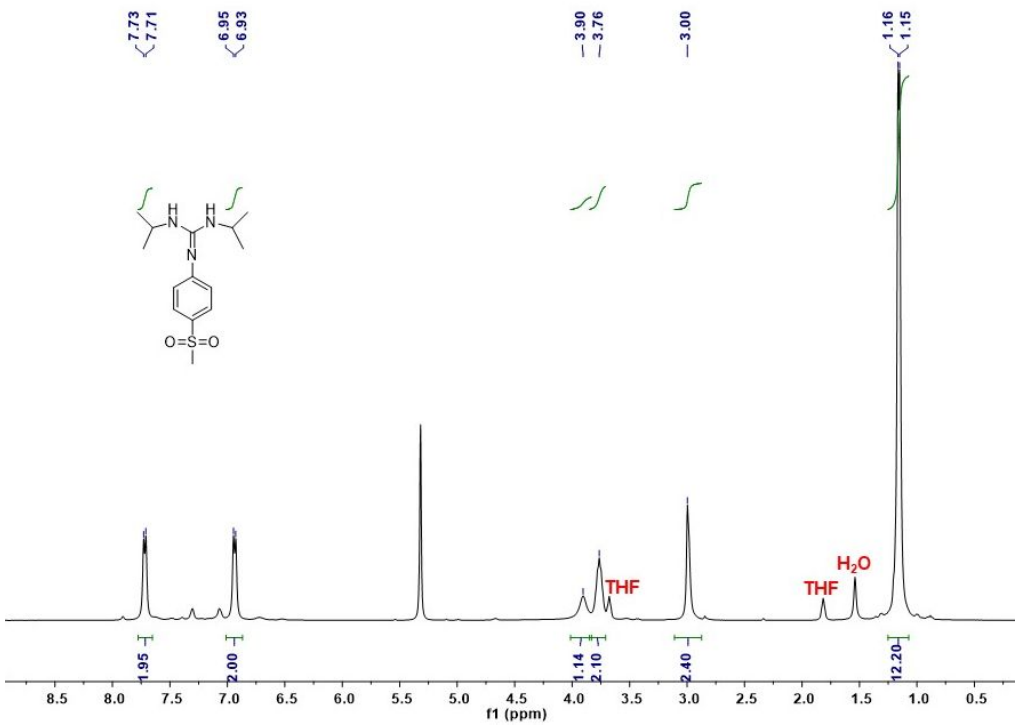


**Figure S45.** $^{1}$H NMR spectrum (400 MHz, 25 °C, $CD_2Cl_2$) of *N*-*p*-methylsulfonylphenyl-*N′, N″*-diisopropylguanidine.

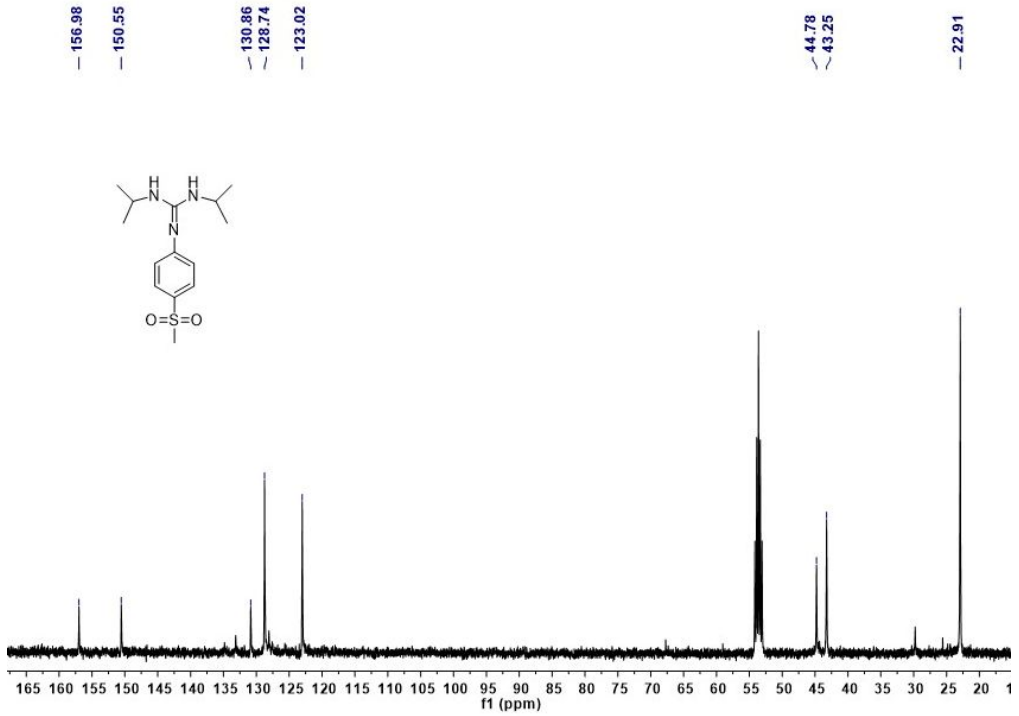


**Figure S46.** $^{13}$C NMR spectrum (101 MHz, 25 °C, $CD_2Cl_2$) of *N*-*p*-methylsulfonylphenyl-*N′, N″*-diisopropylguanidine.

**Supplementary Tables and Schemes**

**Table S1.** Selected bond distances (Å) and angles (deg) in the molecular structures of **1** and **2**.

| | **1** | **2A** | **2B** |
|---|---|---|---|
| Fe-C(carbene) | 2.024(2), 2.013(2) | 2.087(2), 2.081(2) | 2.077(3), 2.084(2) |
| Fe-N(imido) | 1.708(2) | 1.777(2) | 1.779(2) |
| Fe-N(imido)-C1 | 172.3(2) | 172.64(19) | 165.11(7) |
| C-Fe-C | 92.81(9) | 99.12(9) | 98.15(9) |
| Torsion angle ϕ[a] | 66 | 88 | 87 |
| N(imido)-C1 | 1.368(3) | 1.322(3) | 1.332(3) |
| C1-C2 | 1.425(3) | 1.461(3) | 1.456(3) |
| C2-C3 | 1.391(3) | 1.383(4) | 1.382(3) |
| C3-C4 | 1.387(4) | 1.392(4) | 1.391(3) |
| C4-C5 | 1.379(4) | 1.388(4) | 1.395(3) |
| C5-C6 | 1.392(3) | 1.382(3) | 1.385(3) |
| C6-C1 | 1.427(3) | 1.453(3) | 1.450(3) |

[a] Torsion angle ϕ is between the imido Dipp unit and the C(carbene)-Fe-C(carbene) plane.

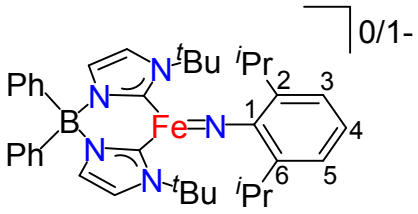


**Table S2.** Key bond distances (Å) and angles (deg) of **2** obtained from X-ray diffraction study and the optimized structure.

| | **2A** | **2B** | Calc. ($S = 2$) |
|---|---|---|---|
| Fe-C(carbene) | 2.087, 2.081 | 2.077, 2.084 | 2.077, 2.074 |
| Fe-N(imido) | 1.777 | 1.779 | 1.782 |
| Fe-N-C | 172.64 | 165.11 | 151.45 |
| C-Fe-C | 99.12 | 98.15 | 95.87 |
| Torsion angle ϕ[a] | 88 | 87 | 80 |

[a] Torsion angle ϕ is between the imido Dipp unit and the C(carbene)-Fe-C(carbene) plane.

**Scheme S1**. Possible mechanism for formation of **4**.

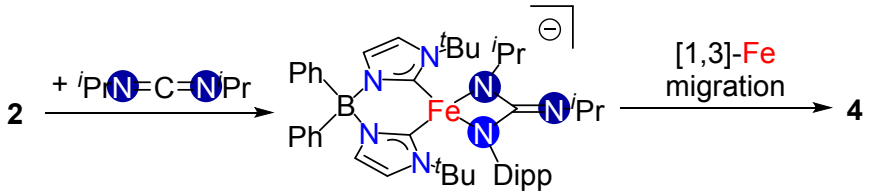

**Computational Details**

Calculations were performed using density functional theory (DFT) as implemented in the Orca 3.0.3 computational software package.[12] Calculations for the anionic part of [$Ph_2B(^tBuIm)_2FeNDipp$][K(18-C-6)$THF_2$] ($S = 2$) was performed with the B3LYP functional and a hybrid def2-TZVP/SVP basis sets.[13] Here, the Fe center, and all atoms attached to Fe were treated with the def2-TZVP basis set for mathematical flexibility. Additionally, Grimme D3BJ dispersion corrections were included for all atoms.[14-15] The COSMO solvation model was employed with the dielectric constant of ε = 7.25 (THF) and the refractive index of 1.407.

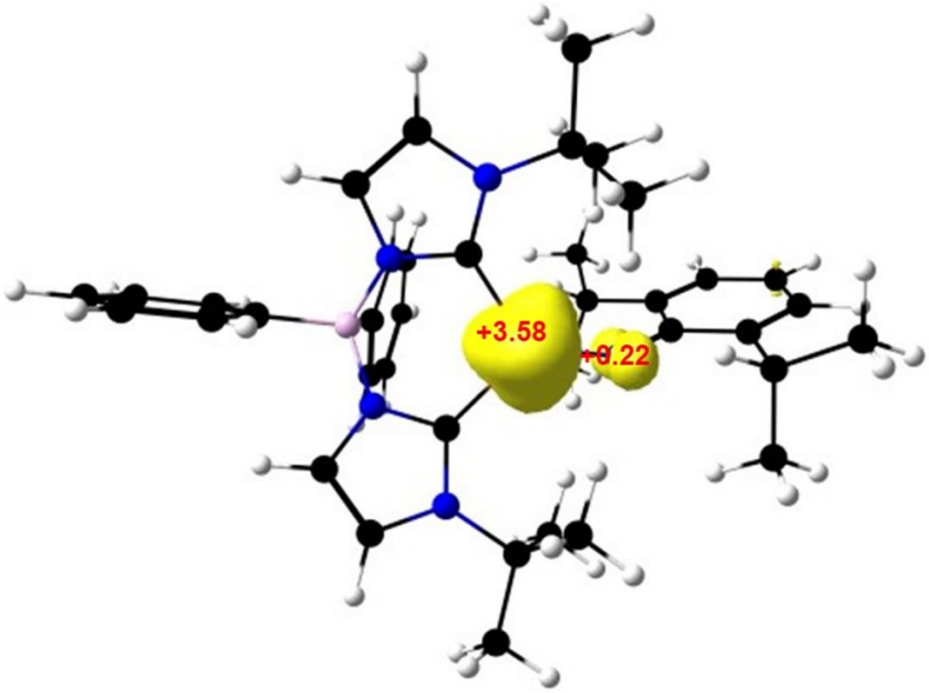


**Figure S47.** Mulliken atomic spin density distribution of [$Ph_2B(^tBuIm)_2FeNDipp$][K(18-C-6)$THF_2$] at its $S = 2$ state with isodensity = 0.01 .

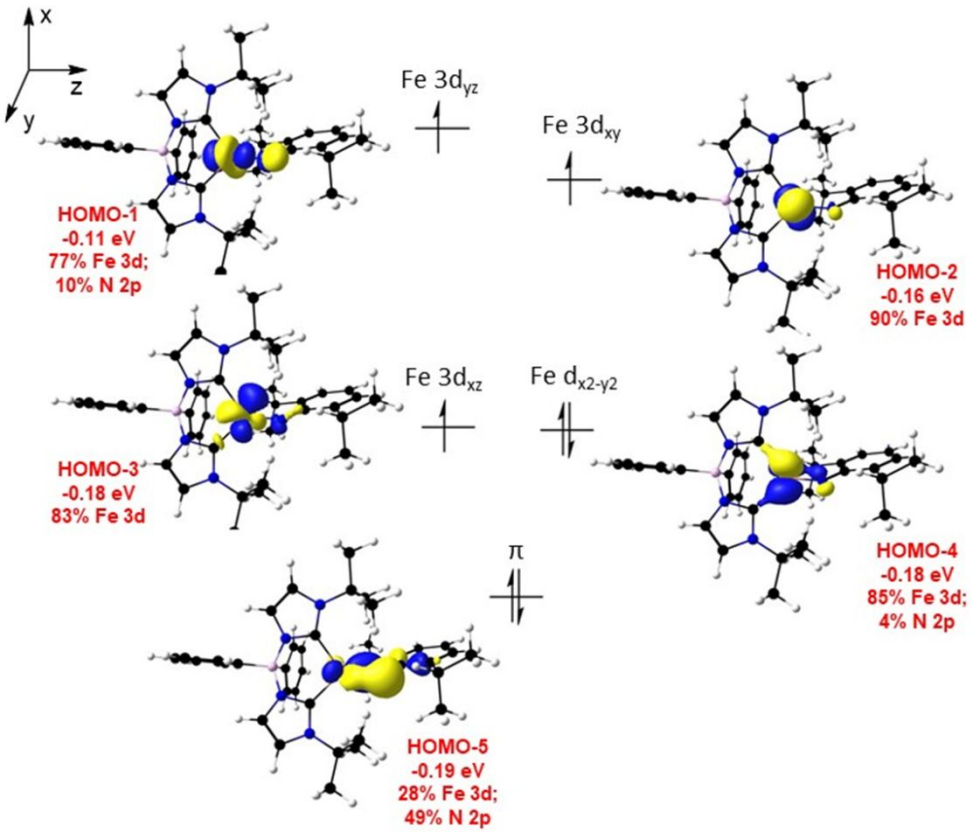


**Figure S48**. Selected frontier orbitals showing of [$Ph_2B(^tBuIm)_2FeNDipp$][K(18-C-6)$THF_2$] ($S$ = 2). Natural orbitals shown with isodensity = 0.05.

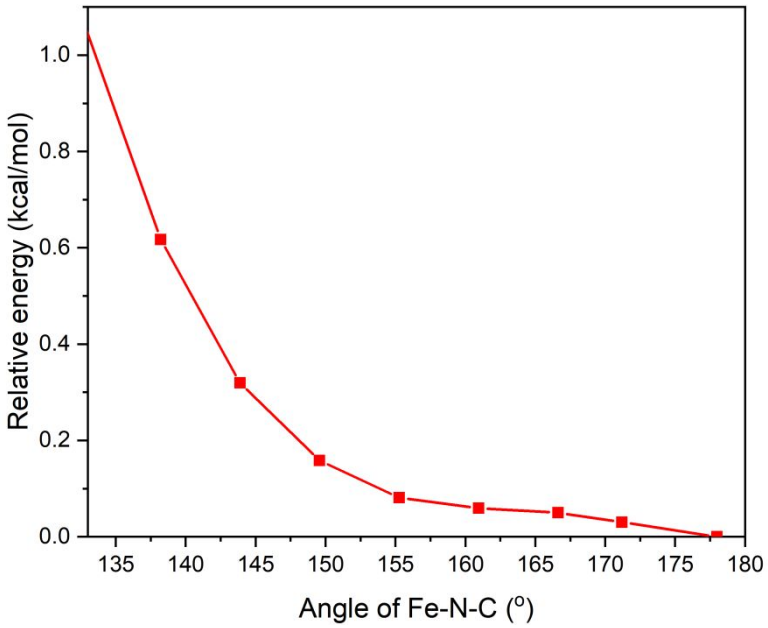


**Figure S49**. Angular dependence of the DFT-calculated single point energy of [$Ph_2B(^tBuIm)_2FeNDipp$][K(18-C-6)$THF_2$] ($S$ = 2) (B3LYP/def2-SVP).

**Crystallographic Information**

[$Ph_2B(^tBuIm)_2FeNDipp$] (**1**)

**Data collection**

The data collection was carried out using Mo Kα radiation (graphite monochromator) with a frame time of 0.75 seconds and a detector distance of 5.00 cm. A collection strategy was calculated and complete data to a resolution of 0.77 Å with a redundancy of 9.7 were collected. Six major sections of frames were collected with 0.50º ω and φ scans. A total of 1849 frames were collected. The total exposure time was 0.40 hours. The frames were integrated with the Bruker SAINT software package[16] using a narrow-frame algorithm. The integration of the data using a monoclinic unit cell yielded a total of 78776 reflections to a maximum θ angle of 27.50° (0.77 Å resolution), of which 7993 were independent (average redundancy 9.856, completeness = 99.7%, $R_{int}$ = 11.91%, $R_{sig}$ = 5.99%) and 5610 (70.19%) were greater than $2\sigma(F^2)$. The final cell constants of a = 16.7241(14) Å, b = 11.7441(9) Å, c = 19.3016(16) Å, β = 112.997(3)°, volume = 3489.7(5) $Å^3$, are based upon the refinement of the XYZ-centroids of 4764 reflections above 20 σ(I) with 4.585° < 2θ < 45.26°. Data were corrected for absorption effects using the Multi-Scan method (SADABS).[17] The ratio of minimum to maximum apparent transmission was 0.906. The calculated minimum and maximum transmission coefficients (based on crystal size) are 0.9770 and 0.9820.

**Structure solution and refinement**

The space group $P2_1/n$ was determined based on intensity statistics and systematic absences. The structure was solved and refined using the SHELX suite of programs.[18] An intrinsic-methods solution was calculated, which provided most non-hydrogen atoms from the E-map. Full-matrix least squares / difference Fourier cycles were performed, which located the remaining non-hydrogen atoms. All non-hydrogen atoms were refined with anisotropic displacement parameters. The hydrogen atoms were placed in ideal positions and refined as riding atoms with relative isotropic displacement parameters. The structure was solved and refined using the Bruker SHELXTL Software Package, using the space group P 1 21/n 1, with Z = 4 for the formula unit, $C_{38}H_{49}BFeN_5$. The final anisotropic fullmatrix least-squares refinement on $F^2$ with 416 variables converged at R1 = 4.76%, for the observed data and wR2 = 11.21% for all data. The goodness-of-fit was 1.093. The largest peak in the final difference electron density synthesis was 0.496 e-/$Å^3$ and the largest hole was -0.480 e-/$Å^3$ with an RMS deviation of 0.075 e-/$Å^3$. On the basis of the final model, the calculated density was 1.223 g/$cm^3$ and F(000), 1372 e-.

**Table S3.** Crystal data and structure refinement for $[Ph_2B(^tBuIm)_2FeNDipp]$.

| | | |
|---|---|---|
| Empirical formula | C38 H49 B Fe N5 | |
| Formula weight | 642.48 | |
| Crystal color, shape, size | black block, 0.05 × 0.04 × 0.04 $mm^3$ | |
| Temperature | 100(2) K | |
| Wavelength | 0.71073 Å | |
| Crystal system, space group | Monoclinic, $P2_1/n$ | |
| Unit cell dimensions | a = 16.7241(14) Å | α = 90°. |
| | b = 11.7441(9) Å | β = 112.997(3)°. |
| | c = 19.3016(16) Å | γ = 90°. |
| Volume | 3489.7(5) $Å^3$ | |
| Z | 4 | |
| Density (calculated) | 1.223 $Mg/m^3$ | |
| Absorption coefficient | 0.466 $mm^{-1}$ | |
| F(000) | 1372 | |
| *Data collection* | | |
| Diffractometer | Venture D8, Bruker | |
| Theta range for data collection | 2.061 to 27.502°. | |
| Index ranges | -21<=h<=21, -15<=k<=14, -24<=l<=25 | |
| Reflections collected | 78776 | |
| Independent reflections | 7993 [$R_{int}$ = 0.1191] | |
| Observed Reflections | 5610 | |
| Completeness to theta = 25.242° | 99.8% | |
| *Solution and Refinement* | | |
| Absorption correction | Semi-empirical from equivalents | |
| Max. and min. transmission | 0.7456 and 0.6752 | |
| Solution | Intrinsic methods | |
| Refinement method | Full-matrix least-squares on $F^2$ | |
| Weighting scheme | $w = [\sigma^2Fo^2 + AP^2 + BP]^{-1}$, with | |
| | $P = (Fo^2 + 2\,Fc^2)/3$, A = 0.0001, B = 5.1887 | |
| Data / restraints / parameters | 7993 / 0 / 416 | |
| Goodness-of-fit on $F^2$ | 1.093 | |
| Final R indices [I>2sigma(I)] | R1 = 0.0476, wR2 = 0.0862 | |
| R indices (all data) | R1 = 0.0827, wR2 = 0.1121 | |
| Largest diff. peak and hole | 0.496 and -0.480 $e.Å^{-3}$ | |

[$Ph_2B(^tBuIm)_2FeNDipp][K(18\text{-}C\text{-}6)THF_2$] (**2**)

**Data collection**

The data collection was carried out using Mo Kα radiation (λ = 0.71073 Å, graphite monochromator) with a frame time of 8 seconds and a detector distance of 60 mm. A collection strategy was calculated and complete data to a resolution of 0.77 Å with a redundancy of 5.6 were collected. The frames were integrated with the Bruker SAINT[19]software package using a narrow frame algorithm. The integration of the data using a monoclinic unit cell yielded a total of 212801 reflections to a maximum θ angle of 25.04° (0.84 Å resolution), of which 22634 were independent (average redundancy 9.402, completeness = 99.9%, $R_{int}$ = 5.32%, $R_{sig}$ = 2.98%) and 18810 (83.11%) were greater than $2\sigma(F^2)$. The final cell constants of a = 19.4416(7) Å, b = 33.4446(12) Å, c = 19.8892(8) Å, β = 97.6220(10)°, volume = 12818.0(8) $Å^3$, are based upon the refinement of the XYZ-centroids of reflections above 20 σ(I).Data were corrected for absorption effects using the Multi-Scan method (SADABS).[20] The calculated minimum and maximum transmission coefficients (based on crystal size) are 0.6828 and 0.7452.

**Structure solution and refinement**

The space group P 1 21/n 1 was determined based on intensity statistics and systematic absences. The structure was solved using the SHELX suite of programs[18] and refined using full-matrix least squares on $F^2$ within the OLEX2 suite.[21] An intrinsic phasing solution was calculated, which provided most non-hydrogen atoms from the E-map. Full-matrix least squares / difference Fourier cycles were performed, which located the remaining non-hydrogen atoms. All non-hydrogen atoms were refined with anisotropic displacement parameters. The hydrogen atoms were placed in ideal positions and refined as riding atoms with relative isotropic displacement parameters. The final full matrix least squares refinement converged to R1 = 0.0523 and wR2 = 0.1143 ($F^2$, all data). The goodness-of-fit was 1.106. On the basis of the final model, the calculated density was 1.204 $g/cm^3$ and F(000), 5008 e-. Disorder was modelled for some of the THF molecules.

**Table S4.** Crystal data and structure refinement for $[Ph_2B(^tBuIm)_2FeNDipp][K(18\text{-}C\text{-}6)THF_2]$.

| | | |
|---|---|---|
| Empirical formula | C124 H194 B2 Fe2 K2 N10 O18 | |
| Formula weight | 2324.40 | |
| Crystal color, shape, size | dark brown block, 0.27 × 0.23 × 0.21 $mm^3$ | |
| Temperature | 100.0 K | |
| Wavelength | 0.71073 Å | |
| Crystal system, space group | Monoclinic, P 1 21/n 1 | |
| Unit cell dimensions | a = 19.4416(7) Å | α = 90°. |
| | b = 33.4446(12) Å | β = 97.6220(10)°. |
| | c = 19.8892(8) Å | γ = 90°. |
| Volume | 12818.0(8) $Å^3$ | |
| Z | 4 | |
| Density (calculated) | 1.204 $Mg/m^3$ | |
| Absorption coefficient | 0.356 $mm^{-1}$ | |
| F(000) | 5008 | |

*Data collection*

| | |
|---|---|
| Diffractometer | Venture D8, Bruker |
| Theta range for data collection | 2.066 to 25.037°. |
| Index ranges | -23<=h<=19, -39<=k<=39, -23<=l<=23 |
| Reflections collected | 264241 |
| Independent reflections | 22636 [$R_{int}$ = 0.0540] |
| Observed Reflections | 19075 |
| Completeness to theta = 25.037° | 99.9% |

*Solution and Refinement*

| | |
|---|---|
| Absorption correction | Semi-empirical from equivalents |
| Max. and min. transmission | 0.7452 and 0.6826 |
| Solution | Intrinsic methods |
| Refinement method | Full-matrix least-squares on $F^2$ |
| Weighting scheme | $w = [\sigma^2Fo^2 + AP^2 + BP]^{-1}$, with |
| | $P = (Fo^2 + 2\,Fc^2)/3$, A = 0.0308, B = 16.258299 |
| Data / restraints / parameters | 22636 / 1740 / 1432 |
| Goodness-of-fit on $F^2$ | 1.106 |
| Final R indices [I>2sigma(I)] | R1 = 0.0523, wR2 = 0.1086 |
| R indices (all data) | R1 = 0.0652, wR2 = 0.1143 |
| Extinction coefficient | n/a |
| Largest diff. peak and hole | 0.539 and -0.551 $e.Å^{-3}$ |

$[Ph_2B(^tBuIm)_2Fe(NHDipp)_2][K(18\text{-}C\text{-}6)THF_2]$ (**3**)

**Data collection**

The data collection was carried out using Mo Kα radiation (λ = 0.71073 Å, graphite monochromator) with a frame time of 1 seconds and a detector distance of 40 mm. A collection strategy was calculated and complete data to a resolution of 0.77 Å with a redundancy of 5 were collected. The frames were integrated with the Bruker SAINT[16]software package using a narrowframe algorithm. The integration of the data using a triclinic unit cell yielded a total of 212627 reflections to a maximum θ angle of 27.48° (0.77 Å resolution), of which 17753 were independent (average redundancy 11.977, completeness = 99.9%, $R_{int}$ = 7.93%, $R_{sig}$ = 3.43%) and 13941 (78.53%) were greater than $2\sigma(F^2)$. The final cell constants of a = 13.7645(9) Å, b = 15.6095(10) Å, c = 20.3195(12) Å, α = 90.363(2)°, β = 98.886(2)°, γ = 115.739(2)°, volume = 3872.2(4) $Å^3$, are based upon the refinement of the XYZ-centroids of 9784 reflections above 20 σ(I) with 4.982° < 2θ < 54.52°. Data were corrected for absorption effects using the Multi-Scan method (SADABS).[17] The ratio of minimum to maximum apparent transmission was 0.959. The calculated minimum and maximum transmission coefficients (based on crystal size) are 0.9060 and 0.9220.

**Structure solution and refinement**

The space group P-1 was determined based on intensity statistics and systematic absences. The structure was solved using the SHELX suite of programs[18] and refined using full-matrix least squares on $F^2$ within the OLEX2 suite.[21] An intrinsic phasing solution was calculated, which provided most non-hydrogen atoms from the E-map. Full-matrix least squares / difference Fourier cycles were performed, which located the remaining non-hydrogen atoms. All non-hydrogen atoms were refined with anisotropic displacement parameters. The hydrogen atoms were placed in ideal positions and refined as riding atoms with relative isotropic displacement parameters. The final full matrix least squares refinement converged to R1 = 0.0525 and wR2 = 0.1567 ($F^2$, all data). The goodness-of-fit was 1.033. On the basis of the final model, the calculated density was 1.164 $g/cm^3$ and F(000), 1472 e-.

**Table S5.** Crystal data and structure refinement for $[Ph_2B(^tBuIm)_2Fe(NHDipp)_2][K(18\text{-}C\text{-}6)THF_2]$.

| | | |
|---|---|---|
| Empirical formula | C76 H122 B Fe K N6 O8.25 | |
| Formula weight | 1357.55 | |
| Crystal color, shape, size | light brown block, 0.33 × 0.28 × 0.27 $mm^3$ | |
| Temperature | 100.0 K | |
| Wavelength | 0.71073 Å | |
| Crystal system, space group | Triclinic, P-1 | |
| Unit cell dimensions | a = 13.7645(9) Å | α = 90.363(2)°. |
| | b = 15.6095(10) Å | β = 98.886(2)°. |
| | c = 20.3195(12) Å | γ = 115.739(2)°. |
| Volume | 3872.2(4) $Å^3$ | |
| Z | 2 | |
| Density (calculated) | 1.164 $g/cm^3$ | |
| Absorption coefficient | 0.304 $mm^{-1}$ | |
| F(000) | 1472 | |
| *Data collection* | | |
| Diffractometer | Venture D8, Bruker | |
| Theta range for data collection | 2.036 to 27.485°. | |
| Index ranges | -17<=h<=17, -20<=k<=20, -26<=l<=26 | |
| Reflections collected | 212627 | |
| Independent reflections | 17753 [$R_{int}$ = 0.0793] | |
| Observed Reflections | 13941 | |
| Completeness to theta = 25.242° | 99.9% | |
| *Solution and Refinement* | | |
| Absorption correction | Semi-empirical from equivalents | |
| Max. and min. transmission | 0.7456 and 0.7148 | |
| Solution | Intrinsic methods | |
| Refinement method | Full-matrix least-squares on $F^2$ | |
| Weighting scheme | $w = [\sigma^2Fo^2 + AP^2 + BP]^{-1}$, with | |
| | $P = (Fo^2 + 2\,Fc^2)/3$, A = 0.0859, B = 3.1177 | |
| Data / restraints / parameters | 17753 / 209 / 896 | |
| Goodness-of-fit on $F^2$ | 1.033 | |
| Final R indices [I>2s(I)] | R1 = 0.0525, wR2 = 0.1448 | |
| R indices (all data) | R1 = 0.0713, wR2 = 0.1567 | |
| Extinction coefficient | n/a | |
| Largest diff. peak and hole | 1.154 and -0.985 $e.Å^{-3}$ | |

[$Ph_2B(^tBuIm)_2Fe(^iPrN)_2CNDipp$][$K(18\text{-}C\text{-}6)THF_2$] (**4**)

**Data collection**

The data collection was carried out using Mo Kα radiation (λ = 0.71073 Å, graphite monochromator) with a frame time of 15 seconds for high angle scans and 2 seconds for low angle scans. The detector distance was 130 mm. A collection strategy was calculated and complete data to a resolution of 0.77 Å with a redundancy of 6.2 were collected. The frames were integrated with the Bruker SAINT[16]software package using a narrow-frame algorithm. The integration of the data using a monoclinic unit cell yielded a total of 201151 reflections to a maximum θ angle of 27.50° (0.77 Å resolution), of which 17171 were independent (average redundancy 11.715, completeness = 99.9%, $R_{int}$ = 8.17%, $R_{sig}$ = 2.95%) and 14705 (85.64%) were greater than $2\sigma(F^2)$. The final cell constants of a = 14.075(5) Å, b = 21.457(7) Å, c = 25.367(8) Å, β = 102.394(7)°, volume = 7482.(4) $Å^3$, are based upon the refinement of the XYZ-centroids of 9640 reflections above 20 σ(I) with 4.813° < 2θ < 54.85°. Data were corrected for absorption effects using the Multi-Scan method (SADABS).[17] The ratio of minimum to maximum apparent transmission was 0.959. The calculated minimum and maximum transmission coefficients (based on crystal size) are 0.8790 and 0.9540.

**Structure solution and refinement**

The space group P 1 21/c 1 was determined based on intensity statistics and systematic absences. The structure was solved using the SHELX suite of programs[18] and refined using full-matrix least squares on $F^2$ within the OLEX2 suite.[21] An intrinsic phasing solution was calculated, which provided most non-hydrogen atoms from the E-map. Full-matrix least squares / difference Fourier cycles were performed, which located the remaining non-hydrogen atoms. All non-hydrogen atoms were refined with anisotropic displacement parameters. The hydrogen atoms were placed in ideal positions and refined as riding atoms with relative isotropic displacement parameters. The final full matrix least squares refinement converged to R1 = 0.0652 and wR2 = 0.1610 ($F^2$, all data). The goodness-of-fit was 1.135. On the basis of the final model, the calculated density was 1.176 $g/cm^3$ and F(000), 2864 e-.

**Table S6.** Crystal data and structure refinement for $[Ph_2B(^tBuIm)_2Fe(^iPrN)_2CNDipp][K(18\text{-}C\text{-}6)THF_2]$.

| | | |
|---|---|---|
| Empirical formula | C71 H115 B Fe K N7 O9.50 | |
| Formula weight | 1324.45 | |
| Crystal color, shape, size | light brown plate, 0.42 × 0.35 × 0.15 $mm^3$ | |
| Temperature | 123 K | |
| Wavelength | 0.71073 Å | |
| Crystal system, space group | Monoclinic, P 1 21/c 1 | |
| Unit cell dimensions | a = 14.075(5) Å | α = 90°. |
| | b = 21.457(7) Å | β = 102.394(7)°. |
| | c = 25.367(8) Å | γ = 90°. |
| Volume | 7483(4) $Å^3$ | |
| Z | 4 | |
| Density (calculated) | 1.176 $g/cm^3$ | |
| Absorption coefficient | 0.314 $mm^{-1}$ | |
| F(000) | 2864 | |
| *Data collection* | | |
| Diffractometer | Venture D8, Bruker | |
| Theta range for data collection | 1.898 to 27.503°. | |
| Index ranges | -18<=h<=18, -27<=k<=27, -32<=l<=32 | |
| Reflections collected | 201151 | |
| Independent reflections | 17171 [$R_{int}$ = 0.0817] | |
| Observed Reflections | 14705 | |
| Completeness to theta = 25.242° | 99.9% | |
| *Solution and Refinement* | | |
| Absorption correction | Semi-empirical from equivalents | |
| Max. and min. transmission | 0.7456 and 0.7154 | |
| Solution | Intrinsic methods | |
| Refinement method | Full-matrix least-squares on $F^2$ | |
| Weighting scheme | $w = [\sigma^2Fo^2 + AP^2 + BP]^{-1}$, with | |
| | $P = (Fo^2 + 2\,Fc^2)/3$, A = 0.0676, B = 9.1596 | |
| Data / restraints / parameters | 17171 / 438 / 821 | |
| Goodness-of-fit on $F^2$ | 1.135 | |
| Final R indices [I>2s(I)] | R1 = 0.0652, wR2 = 0.1552 | |
| R indices (all data) | R1 = 0.0770, wR2 = 0.1610 | |
| Extinction coefficient | n/a | |
| Largest diff. peak and hole | 0.758 and -0.689 $e.Å^{-3}$ | |

**References**


1. Schwindt, M. A.; Lejon, T.; Hegedus, L. S. *Organometallics* **1990**, *9*, 2814.
2. Hickey, A. K.; Lee, W. T.; Chen, C. H.; Pink, M.; Smith, J. M. *Organometallics* **2016**, *35*, 3069.
3. Zhao, Y. M.; Nguyen, H.; Male, L.; Craven, P.; Buckley, B. R.; Fossey, J. S. *Organometallics* **2018**, *37*, 4224.
4. Lichtscheidl, A. G.; Janicke, M. T.; Scott, B. L.; Nelson, A. T.; Kiplinger, J. L. *Dalton Trans.* **2015**, *44*, 16156.
5. Evans, D. F. *J. Chem. Soc.* **1959**, 2003.
6. Ion Prisecaru, WMOSS4 Mössbauer Spectral Analysis Software, www.wmoss.org, 2009-2016.
7. Vardhanapu, P. K.; Bheemireddy, V.; Bhunia, M.; Vijaykumar, G.; Mandal, S. K. *Organometallics* **2018**, *37*, 2602.
8. Lachs, J. R.; Barrett, A. G. M.; Crimmin, M. R.; Kociok-Köhn, G.; Hill, M. S.; Mahon, M. F.; Procopiou, P. A. *Eur. J. Inorg. Chem.* **2008**, 4173.
9. Bhattacharjee, J.; Harinath, A.; Banerjee, I.; Nayek, H. P.; Panda, T. K. *Inorg. Chem.* **2018**, *57*, 12610.
10. Pottabathula, S.; Royo, B. *Tetrahedron Lett.* **2012**, *53*, 5156.
11. Zhao, B.; Xiao, Y.; Yuan, D.; Lu, C. R.; Yao, Y. M. *Dalton Trans.* **2016**, *45*, 3880.
12. Neese, F. *WIREs Comput. Mol. Sci.* **2012**, *2*, 73.
13. Pantazis, D. A.; Chen, X. Y; Landis, C. R.; Neese, F. *J. Chem. Theory Comput.* **2008**, *4*, 908.
14. Grimme, S.; Ehrlich, S.; Goerigk, L. *J. Comput. Chem.* **2011**, *32*, 1456.
15. Grimme, S.; Antony, J.; Ehrlich, S.; Krieg, H. *J. Chem. Phys.* **2010**, *132*, 154104.
16. SAINT v. 2018.1, Bruker AXS, Madison, WI, 2018.
17. SADABS v. 2018.1, Bruker AXS, Madison, WI, 2018.
18. Sheldrick, G. M. *Acta Cryst.* **2008**, *A64*, 112.
19. SAINT, V8.30A, Bruker Analytical X-Ray Systems, Madison, WI, 2012.
20. SADABS, 2.03, Bruker Analytical X-Ray Systems, Madison, WI, 2016.
21. Dolomanov, O. V.; Bourhis, L. J.; Gildea, R. J.; Howard, J. A. K.; Puschmann, H. *J. Appl. Crystallogr.* **2009**, *42*, 339.